Cellulose (2023) 30:2627–2652
https://doi.org/10.1007/s10570-022-05033-3

ORIGINAL RESEARCH

Flame-retardant finishing of cotton fabrics using DOPO functionalized alkoxy- and amido alkoxysilane

Wael Ali · Olga Zilke · Dominic Danielsiek · Alaa Salma · Bassem Assfour · Valbone Shabani · Seden Caglar · Hung Minh Phan · Leonie Kamps · Ruth Wallmeier · Ying Feng · Torsten Textor · Jochen S. Gutmann · Thomas Mayer-Gall

Received: 19 August 2022 / Accepted: 26 December 2022 / Published online: 4 January 2023

Abstract In the present study, DOPO-based alkoxysilane (DOPO-ETES) and amido alkoxysilane (DOPO-AmdPTES) were synthesized by one-step and without by-products as halogen-free flame retardants. The flame retardants were applied on cotton fabric utilizing sol–gel method and pad-dry-cure finishing process. The flame retardancy, the thermal stability and the combustion ehaviour of treated cotton were evaluated by surface and bottom edge ignition flame test (according to EN ISO 15025), thermogravimetric analysis (TGA) and micro-scale combustion calorimeter (MCC). Unlike CO/DOPO-ETES sample, cotton treated with DOPO-AmdPTES nanosols exhibits self-extinguishing ehaviour with high char residue, an improvement of the LOI value and a significant reduction of the PHRR, HRC and THR compared to pristine cotton. Cotton finished with DOPO-AmdPTES reveals a semi-durability after ten laundering cycles keeping the flame-retardant properties unchanged. According to the results obtained from TGA-FTIR, Py-GC/MS and XPS, the major activity of flame retardant occurs in the condensed phase via catalytic induced char formation as physical barrier along with the activity in the gas phase derived mainly from the dilution effect. The early degradation of CO/DOPO-AmdPTES compared to CO/DOPO-ETES, triggered by the cleavage of the

Supplementary Information The online version contains supplementary material available at https://doi.org/10.1007/s10570-022-05033-3.

W. Ali (✉) · O. Zilke · D. Danielsiek · A. Salma · V. Shabani · H. M. Phan · L. Kamps · R. Wallmeier · J. S. Gutmann (✉) · T. Mayer-Gall (✉)
Deutsches Textilforschungszentrum Nord-West gGmbH, Adlerstr. 1, 47798 Krefeld, Germany
e-mail: ali@dtnw.de; wael.ali@uni-due.de

J. S. Gutmann
e-mail: jochen.gutmann@uni-due.de

T. Mayer-Gall
e-mail: myer-gall@dtnw.de

W. Ali · V. Shabani · S. Caglar · Y. Feng · J. S. Gutmann · T. Mayer-Gall
Institute of Physical Chemistry, University of Duisburg-Essen, Duisburg-Essen, Universitätsstraße 2, 45117 Essen, Germany

B. Assfour
Department of Chemistry, Atomic Energy Commission, P. O. Box, 6091 Damascus, Syria

T. Textor
Texoversum School of Textiles, Reutlingen University, Alteburgstraße 150, 72762 Reutlingen, Germany

J. S. Gutmann · T. Mayer-Gall
Center for Nanointegration Duisburg-Essen (CENIDE), Carl-Benz-Straße 199, 47048 Duisburg, Germany

weak bond between P and C=O, as the DFT study indicated, provides the beneficial effect of this flame retardant on the fire resistance of cellulose.

Graphical abstract

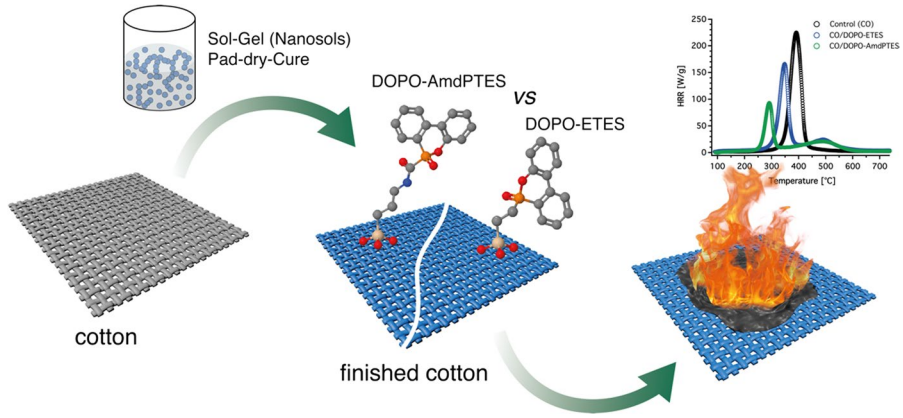

Keywords Flame retardant · DOPO · Sol–gel · Textile finishing · Semi-durable treatment

Introduction

Restricting and banning of halogenated flame retardants over the last two decades moved the researchers and manufacturers towards various alternatives to meet the governmental regulations and laws in regard to human security, environmental impact and sustainability (Lu and Hamerton 2002). Among those alternatives, phosphorus containing flame retardants (FRs) play a crucial role, providing gas-phase activity similar to halogenated substances (Schartel 2010). Depending on the phosphorus oxidation state, their thermal decomposition into PO and PO_2 radicals enables high energy H and OH radicals to be captured, causing a decrease of heat release and thus, halting flame propagation (Kundu et al. 2020b). Throughout the investigation of organophosphorus FRs, the phosphinic acid ester 9, 10-dihydro-9-oxa-10-phosphaphenanthrene-10-oxide (DOPO) and its derivatives became the focal point of interest (Saito 1972; Liang et al. 2012; Zhang and Yang 2011; Wu et al. 2020). Showing excellent fire retardation properties for polymers, such as highly flammable polyurethane foam (König and Kroke 2012) or intensely smoke producing epoxy resins (Bifulco et al. 2022; Schäfer et al. 2007; Yu et al. 2010; Zhang et al. 2020a; Peng et al. 2016; Qian et al. 2013), DOPO-derivatives have proven to be valuable additives in various polymer and composite related applications (Gu et al. 2020; Chen et al. 2014; Zhang et al. 2016a, b; Qian et al. 2012). As Zhang et al. demonstrated, DOPO-derivatives can effectively introduce flame-retarding properties to epoxy resins in add-ons as low as 2.5 wt.%, increasing LOI and promoting a self-extinguishing effect in the UL-94 test (Zhang et al. 2011). The low add-on required for a flame retarding effect qualifies DOPO and its derivatives to be implemented into high-performance composite materials, such as carbon fibre reinforced epoxy resins for aviation (Perret et al. 2011b) as well as automotive applications (Perret et al. 2011a) or silver nanowire reinforced epoxy composites with enhanced thermal conductivity (Feng et al. 2018). Likewise, DOPO-derivatives can be added to polymer blends for melt-spun synthetic fibers (Vasiljević et al. 2019), be introduced as a comonomer into the polymerization reaction of polyamide 6, yielding an intrinsic flame-retardant yarn(Čolovićet al. 2021) or be UV-grafted onto synthetic fibre surfaces (Kundu et al. 2017). The synthetic versatility of DOPO to form various flame-retardant additives can further be underlined by examples of DOPO-substituted pentaerithrol and cyanuric acid derivatives (Müller et al. 2013), just to name two of the most prominent DOPO-based FR in recent literature. As for most textile applications, a treatment of semi-finished products is preferred,

which needs to fulfill high demands regarding the treatment procedure (i.e., use of water/non-toxic solvents), unadulterated optical appearance and feel, as well as durability (washing, weathering, UV-resistance) (Salmeia et al. 2016; Nazir et al. 2021). Hence, a chemical immobilization of the FR on the textile surface is required, which can be achieved using different approaches including UV-curable FRs (Mayer-Gall et al. 2015), sol–gel technique (Wang et al. 2016; Kanat and Eren 2019; Zhang et al. 2020b) and crosslinking reaction between ammonium phosphate groups and cellulose using dicyandiamide as catalyst (Gu et al. 2021; Chen et al. 2022). Recently, a new methodology has been reported on the formation of physical networks via in-situ crosslinking reaction to produce a durable (Nazir et al. 2021) or semi-durable (Zilke et al. 2022) flame-retardant finishing. The utilization of DOPO-based silans and their application via pad-dry-cure procedure has previously been demonstrated for cotton (Hu et al. 2011), polyester (Wang et al. 2011), silk (Liu et al. 2018), and polyamide (Šehić et al. 2016; Kundu et al. 2020a) textiles. For polyamide and cotton, DOPO-ethyl trialkoxysilane (DOPO-ETMS/-ETES) are among the most frequently investigated silane-based flame-retardants (Kundu et al. 2020b; Sahyoun et al. 2015; Chernyy et al. 2015; Vasiljević et al. 2015). Chernyy et al. reported a synergistic effect between P an Si regarding char formation, however, during vertical flammability tests, high loads of DOPO-ETMS were required to achieve sufficient flame suppression (Chernyy et al. 2015). Similar results have been reported by Vasiljević et al., attributing the flame retarding mechanism of DOPO-ETMS to the aforementioned radical scavenging gas-phase activity, as well as the solid phase phosphorylation of cellulose which, in synergy with the formation of silicon oxide, builds up a protective char layer on the substrates surface (Vasiljević et al. 2015). On the contrary, the high thermal degradation temperature of DOPO-ETMS results in a late onset of the flame retarding response, thus limiting the FRs effectiveness (Qian et al. 2012).

Herein we report the synthesis of a novel DOPO-based silane, containing an additional amido functionality, which shows an overall increased performance in terms of flame retardation and protective char formation, compared to the literature-renowned reference, DOPO-ETES. The investigated flame-retardant finishing was applied to cotton and the coated cotton fabrics were characterized. The thermal stability, fire retardancy, pyrolysis behavior in both gas and condensed phase, as well as corresponding flame-retardant mechanism were also investigated.

Experimental

Materials

Commercial woven cotton fabric (CO, plain weave, 170 g/m^2, white) was purchased from wfk Testgewebe GmbH, Brüggen, Germany. 9,10-Dihydro-9-oxa-10-phosphaphenanthrene-10-oxid (DOPO, 97%) was purchased from TCI Europe N.V. (Zwijndrecht, Belgium). Vinyltriethoxysilane (VTES, 98%) and 3-isocyanatopropyltriethoxysilane (ICPTES, 95%) were purchased from abcr GmbH (Karlsruhe, Germany). 2,2´-Azobis(2-methylpropionitrile) (AIBN, 97%) and triethylamin (Et_3N, 99%) were purchased from Merck KGaA (Darmstadt, Germany). Tetrahydrofuran (THF, 99.9%), dichloromethane (DCM, 99.9%) and ethanol (EtOH, 99.8%) were purchased from Fisher Scientific GmbH (Schwerte, Germany). Before use, THF and DCM were dried using molecular sieve 4 Å purchased from Sigma Aldrich (St. Louis, USA).

It should be noted that the flame retardant, DOPO-ethyltriethoxysilane (DOPO-ETES), was prepared similarly as described elsewhere (Vasiljević et al. 2015), and the new compound, DOPO-amidopropyltriethoxysilane (DOPO-AmdPTES) was prepared in small quantity in our lab. The production of both FRs were scaled up and donated by abcr GmbH (Karlsruhe, Germany) with the article numbers AB582754 and AB582755.

Synthesis and characterization of flame retardants

Synthesis of DOPO-ethyltriethoxysilane (DOPO-ETES)

As we stated above, the DOPO-ETES flame retardant was prepared similarly as described elsewhere (Vasiljević et al. 2015). Typically, 20.65 g of DOPO (96 mmol, 1 eq.) was dissolved in 100 mL dry THF at 80 °C in a 250 mL two-necked round-bottom flask with a magnetic stirrer, reflux condenser and nitrogen inlet. After complete solubilization of DOPO,

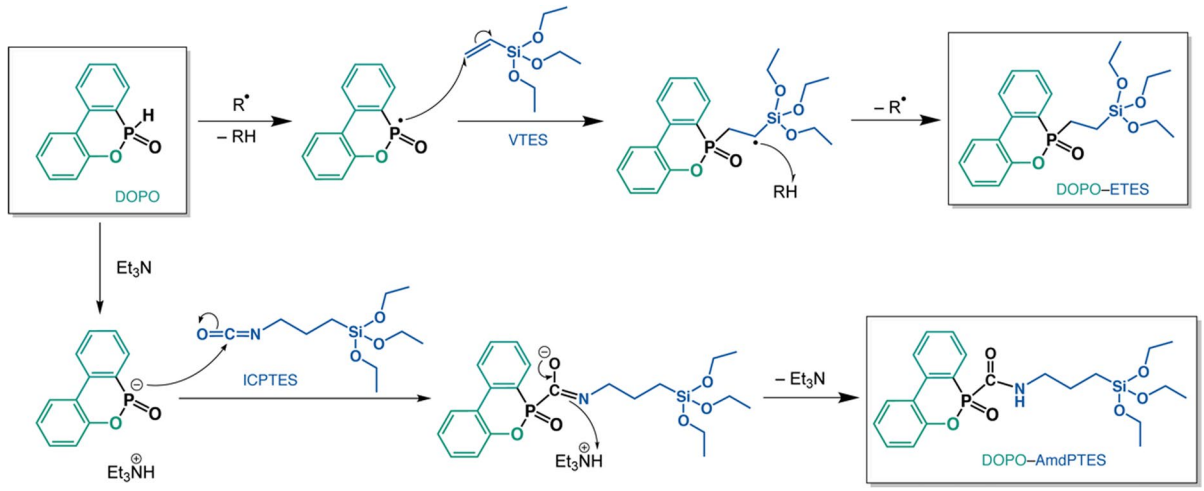

Scheme 1 Synthesis and mechanism route of DOPO-ETES and DOPO-AmdPTES

27.27 g of vinyltrietoxysilane (VTES) (96 mmol, 1 eq.) was added and the mixture was stirred for 15 min under saturated nitrogen atmosphere. 0.80 g of AIBN (5 mmol, 0.05 eq.) predissolved in 50 mL dry THF was slowly added into the reaction vessel and kept overnight at 80 °C. The product was purified by removing the solvent using a rotary evaporator yielding a light-yellow liquid product (95% yield). The schematic process of the reaction mechanism is presented in Scheme 1. The structure of DOPO-ETES was confirmed by NMR, FT-IR and ESI–MS (see supplementary information, Fig. S2, S3, S4 and S5).

^{1}H-NMR (300 MHz, $CDCl_3$): δ [ppm] = 0.83 (m, 2H, CH_2–Si), 1.15 & 1.22 (t, J = 7 Hz, 9H, CH_3), 2.07 (m, 2H, CH_2–P), 3.73 (m, 6H, CH_2–O), 7.20 (d, J = 7.7 Hz, 1H, CH_{Ar}), 7.23 (t, J = 6.7 Hz, 1H, CH_{Ar}), 7.36 (t, J = 7.7 Hz, 1H, CH_{Ar}), 7.49 (td, J = 2.9, 7.4 Hz, 1H, CH_{Ar}), 7.68 (td, J = 1.1, 7.5 Hz, 1H, CH_{Ar}), 7.82 (dd, J = 0.9, 7.5 Hz, CH_{Ar}), 7.89 (d, J = 8.2 Hz, 1H, CH_{Ar}), 7.93 (d, J = 7.9 Hz, 1H, CH_{Ar}).

^{13}C-NMR (75 MHz, $CDCl_3$): δ [ppm] = 1.87 (d, CH_2–Si), 18.32 (s, CH_3), 22.57 (s, CH_2), 58.72 (s, CH_2–O), 120.52 (d, CH_{Ar}), 122.37 (d, C–P, C_q), 123.91 (d, CH_{Ar}), 124.58 (s, CH_{Ar}), 125.25 (s, CH_{Ar}), 128.40 (d, CH_{Ar}), 130.15 (d, CH_{Ar}), 130.63 (s, CH_{Ar}), 133.21 (d, CH_{Ar}), 135.93 (d, C_q), 137.14 (s, C_q), 149.31 (d, C_q).

^{31}P-NMR (122 MHz, $CDCl_3$): δ [ppm] = 39.66 (s, 1P).

FT-IR (ATR) [cm^{-1}]: 780 (Ar C–H, sp^2, bend), 910 (P–O–Ph), 1078 (Si–O), 1195 (alkoxy C–O), 1274 (P=O), 1432 (C–H, sp^3, bend), 1478 (P–Ph), 1595 (Ar C=C, P–Ph), 2924 (C–H, sp^3, stretch), 3066 (C–H, sp^2, stretch).

High Resolution ESI–MS: calculated for m/z $[M+Na]^+$: 429.1258, found: 429.1262.

Synthesis of DOPO-amidopropyltriethoxysilane (DOPO-AmdPTES)

In a typical experiment, dry DCM (100 mL), DOPO (21.62 g, 100 mmol, 1 eq.), ICPTES (23.99 g, 100 mmol, 1 eq.) and TEA (400 mg, 4 mmol) as a catalyst were charged to a tow-necked round-bottom flask with a magnetic stirrer and nitrogen inlet. The reaction solution was purged for 20 min with nitrogen and sealed under nitrogen. The reaction was carried out overnight at room temperature under stirring. The product was purified by removing the solvent using a rotary evaporator yielding a white solid product (41.6 g, 99% yield). The schematic process of the reaction mechanism is presented in Scheme 1. The structure of DOPO-AmdPTES was also confirmed by NMR, FT-IR and ESI–MS (see supplementary information, Fig. S6, S7, S8 and S9) ^{1}H-NMR (300 MHz, $CDCl_3$): δ [ppm] = 0.67 (t, J = 7.5 Hz 2H, CH_2–Si), 1.24 (t, J = 7 Hz, 9H, CH_3), 1.74 (quint, J = 7.5 Hz, 2H, CH_2), 3.37 (q, J = 7.5 Hz, 2H, CH_2–NH), 3.82 (q, J = 7 Hz, 6H, CH_2–O), 7.23 (d, J = 7.5 Hz, 1H, CH_{Ar}), 7.26 (t, J = 7 Hz, 1H, CHAr), 7.37 (t, J = 7.5 Hz, 1H, CHAr), 7.52 (td, J = 1.1, 7.5 Hz, 1 H, CH_{Ar}), 7.75

(td, J = 1.1, 7.5 Hz, 1H, CH_{Ar}), 7.90 (dd, J = 1.2, 8 Hz, 1H, CH_{Ar}), 7.96 (d, J = 8.1 Hz, 1H, CH_{Ar}), 8.02 (d, J = 7.9 Hz, 1H, CH_{Ar}).

^{13}C-NMR (75 MHz, $CDCl_3$): δ [ppm] = 7.75 (s, CH_2–Si), 18.26 (s, CH_3), 22.70 (s, CH_2), 42.04 (d, CH_2), 58.41 (s, CH_2–O), 119.94 (d, CH_{Ar}), 121.12 (d, C–P, C_q), 121.55 (s, C_q), 123.62 (d, CH_{Ar}), 124.70 (d, CH_{Ar}), 128.42 (d, CH_{Ar}), 130.64 (s, CH_{Ar}), 130.80 (d, CH_{Ar}), 134.31 (d, CH_{Ar}), 137.21 (d, CH_{Ar}), 149.72 (d, C_q), 165.39 (s, C–O, C_q), 167.64 (s, C=O, C_q).

^{31}-P NMR (122 MHz, $CDCl_3$): δ [ppm] = 12.11 (s, 1P).

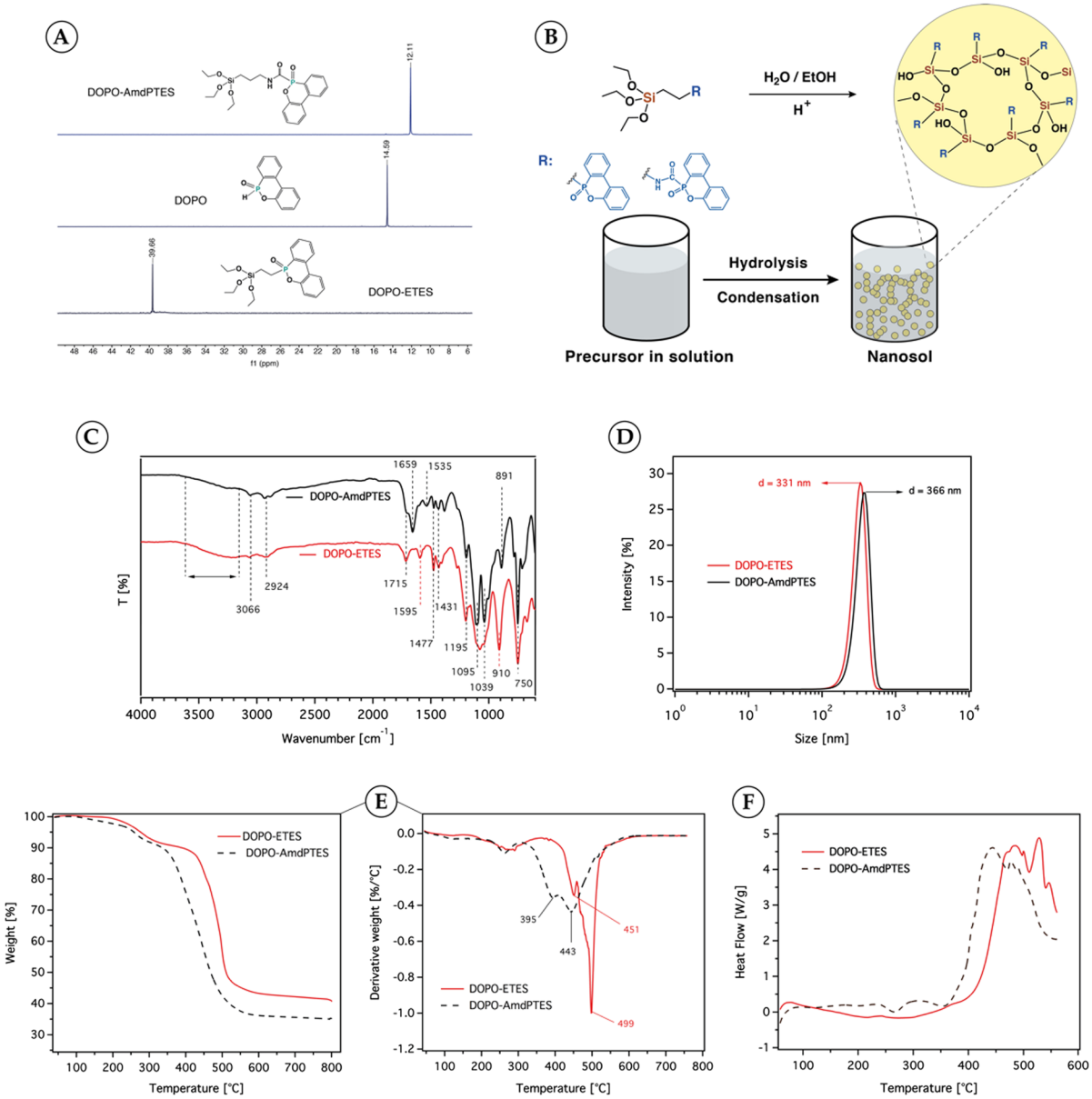

Fig. 1 (**A**) ^{31}P-NMR of DOPO, DOPO-ETES and DOPO-AmdPTES compounds. (**B**) nanosol formation, (**C**) FTIR spectra, (**D**) particle size distribution measured by DLS, (**E**) TGA and DTG curves measured under a N_2 atmosphere and (**F**) DSC curves of both flame-retardant polymers

FT-IR (ATR) [cm^{-1}]: 780 (Ar C–H, sp^2, bend), 937 (P–O–Ph), 1073 (Si–O), 1195 (alkoxy C–O), 1255 (P=O), 1432 (C–H, sp^3, bend), 1478 (P–Ph), 1521 (Ar C=C, P–Ph), 1654 (N–C=O), 2883 (C–H, sp^3, stretch), 2974 (C–H, sp^2, stretch), 3256 (2° N–H).

High Resolution ESI–MS: calculated for m/z $[M+Na]^+$: 486.1472, found: 486.1486.

Sol–gel coating protocol

For the sol–gel coating on the studied fabric, sol solutions were first prepared via dissolving the precursors silane into a mixture of water and ethanol (v/v, 1:1) at three different concentrations. The pH of the sol solutions was adjusted to 4–5 with a few drops of concentrated acetic acid (Fig. 1C). The mixture was stirred for 72 h prior to the coating procedure. The sol solution was applied to the fabric samples by the pad-dry-cure method using a simple standard laboratory padding machine and an oven. This includes full immersion at room temperature for 10 min followed by a wet pick-up, drying and curing at 130 °C for 20 min. The samples were then rinsed with tap water for 5 min to remove excess materials. The washed fabric was dried at ambient conditions. To determine the loading of flame retardants, the weight of samples was recorded before and after the sol application. The samples were left for 24 h under standard atmospheric conditions (60 ± 2% relative humidity and 20 ± 1 °C) prior to weight measurement. The mass add-on value (%) was calculated using the following equation:

$$\text{Add-on}\,(\%) = (m_1 - m_0)/m_0 \times 100 \quad (1)$$

where m_0 and m_1 correspond to the weights of the fabric pieces before and after sol finishing.

Measurement and characterization

Proton, carbon and phosphor nuclear magnetic resonance (^{1}H-, ^{13}C- and ^{31}P-NMR) analyses were recorded on a Bruker DMX-300 instrument (Bremen, Germany) at 75, 122 and 300 MHz, respectively, using deuterated chloroform ($CDCl_3$) solvent. The chemical shifts were reported in part per million (ppm). Spin multiplicity is shown by s = singlet, d = doublet, t = triplet, q = quartet, quint = quintet.

Fourier transform infrared spectroscopy (FT-IR) spectra were acquired using an IR Prestige-21 (Shimadzu Deutschland GmbH, Duisburg, Germany) at the attenuated total reflection (ATR) mode in the range of 600–4000 cm^{-1} with an average of 32 scans. A golden gate equipped with a diamond crystal (Specac Ltd, Orpington, UK) and resolution of 4 cm^{-1} was used.

Thermogravimetric analyses (TGA) analyses were performed using Discovery TGA 55 (TA Instruments, Hüllhorst, Germany) from 40 to 800 °C. Approximately 10 mg of dried sample (24 h at 60 °C) was placed in a platinum crucible. The temperature was first held at 40 °C for 5 min to erase the thermal history and then heated at the heating rate of 20 °C/min under both air and nitrogen atmosphere with a gas flow rate of 90 mL/min. To analyze the smoke gases released during the decomposition, TGA was coupled with the FT-IR spectrometer described above via gas cell.

Differential Scanning Calorimetry (DSC) analyses were carried out using a DSC Q20 (TA Instruments, New Castle, USA) calorimeter under N_2 as purge gas with a flow rate of 50 mL/min. Each sample (~ 4 mg) was placed into a perforated aluminum pan and the thermal properties were recorded between 50 °C and 600 °C with a heating rate of 20 °C/min. The samples were dried for 24 h at 60 °C prior to analysis.

Micro-scale combustion calorimeter (MCC) measurements were conducted using a Fire Testing Technology Ltd. (East Grinstead, UK) following ASTM D 7309 Method A. For each run, the sample was first pyrolyzed up to 750 °C with a heating rate of 1 °C/s in a stream of N_2 flowing at a rate of 80 mL/min. Then the obtained volatile thermal degradation products were combusted at 900 °C in a combustion chamber after mixing with a stream of pure O_2 at a flow rate of 20 mL/min. The recorded data were analyzed using Origin 2018b software (OriginLab Cooperation, Northampton, USA). Each sample was run in triplicate and the values obtained are average of three measurements.

Pyrolytic degradation products were analyzed using a TDS-GC/MS system with a pyrolysis module PM1 (Agilent Technologies model GC 7890B MSF 5977B, TDS 3 and PM1, Gerstel GmbH & Co. KG, Mühlheim an der Ruhr, Germany). The textile samples were pyrolyzed for 1 min at 700 °C in a sample tube placed in the thermal desorption system (TDS). The temperature of the cooled injection system (CIS) was set at − 50 °C. With a heating rate of 12 °C/s the

cryofocused pyrolysis products were heated to 300 °C and introduced into the GC with He as a carrier gas. The pyrolysis mixture was separated in a capillary column (HP Ultra 2) with a heating rate of 10 °C/min starting from 50 to 300 °C. Analytes were ionized by electron ionization (EI) at 70 eV and scanned in the positive mode in the mass range of m/z 35–620. Data were analyzed using OpenChrom (Wenig and Odermatt 2010) and compounds were identified by the utilization of NIST Standard Reference Database Number 69 (William 2022), MassBank (Schulze 2006), and SpectraBase (Wiley and Sons 2000). Peak areas were determined using Agilent MassHunter.

Scanning electron microscopy was performed using an S-3400 N II SEM (Hitachi HighTech Europe GmbH, Mannheim, Germany) operated at an accelerating voltage of 10 kV. The surface of the samples was sputtered with gold in vacuum for 4 min using a Quorum Emitech K500X sputter coater (Ashford, Kent, UK).

X-ray photoelectron spectroscopy (XPS) measurements were conducted using a PHI 5000 Versaprobe II. Monochromatic Al-anode with a *Kα* line at 1486.6 eV was utilized with a beam size of 100 µm, dual beam charge neutralization and an electron emission angle of 45°. The recorded XPS spectra were corrected to the C1s signal of 284.8 eV (related to hydrocarbons) and fitted using a baseline correction of Shirley function and Voigt line profile by mean of Casa XPS software.

Dynamic light scattering (DLS) was performed to determine the size distribution of the sol nanoparticles using a Zetasizer 1000 apparatus (Malvern Panalytical Ltd, Malvern, UK). The sample was diluted by a factor of 1000 to minimize the agglomeration. Measurements were conducted at an angle of 90° and a temperature of 25 °C.

Flame tests were performed according to EN ISO 15025:2016 (protective clothing-protection against heat and flame-method of test for limited flame spread, 10 s ignition) using Gester flammability tester (Model GT-C35B) following both procedures, A for surface ignition (flame height 25 mm) and B for bottom edge ignition (30°, flame height 40 mm). Passing requirements were assessed following ISO 11611:2015. The limiting oxygen index (LOI) was determined by igniting 5 samples with dimension of 5 × 10 cm according to ISO 4589-2. The flame was applied to the upper edge of the samples in a glass tube containing O_2/N_2 mixture.

The washing durability of finished cotton samples was assessed by measuring the weight loss (%) and the phosphorus content (%) after 1, 3, 5 and 10 washing cycles using a linitester devise (Heraeus-Original Hanau, Germany) according to ISO 105-C08:2010 at 40 °C using ECE non-phosphate detergent.

Theoretical calculation

The main goal of the modelling work is to try to understand the mechanism of flame-retardants degradation under escalated temperature. To this end, molecular dynamic simulations using the DFTB + simulation package were performed (Hourahine et al. 2020). The 3ob-3-1 parameter sets were used (Gaus et al. 2014). Firstly, the experimental structures of the two molecules were relaxed using geometry optimization tool. Grimme's DFT-D3 method was employed to account for dispersion correction. The relaxed structures were employed for equilibration via MD simulation. Structures were equilibrated at 300 K for 10 ps, followed by an NVT ensemble simulation at 400, 500, 600 and 700 K. The time step of MD simulation is 0.5 fs with a duration 20 ps at each temperature. The bond lengths of each system were evaluated over the temperature range between 25 and 800 K, and within 20 temperature steps.

Results and discussion

Characterization of DOPO-ETES and DOPO-AmdPTES nanosols

As shown in Scheme 1, the DOPO-based FRs were prepared by the P–H addition of DOPO to the double bond in VTES or to the isocyanate functional group in ICPTES. The formation of DOPO-ETES and DOPO-AmdPTES are proven by the disappearance of the P–H characteristic peak in DOPO, which can be confirmed with ^{1}H-NMR, ^{31}P-NMR and FTIR techniques. Specifically, the signal peak observed in the ^{31}P-NMR spectra for both FRs with a chemical shift from $\delta = 14.59$ ppm of pure DOPO to $\delta = 39.66$ ppm for DOPO-ETES and $\delta = 12.11$ ppm for DOPO-AmdPTES confirms the complete reaction

of DOPO (Fig. 1A). The ^{1}H-NMR spectra of both FRs are shown in Fig. S2 and S6, respectively. The disappearance of the P–H peak at δ = 8.77 ppm of DOPO (Fig. S1) are clearly indicative of the FRs formation. Besides, the ^{13}C-NMR spectra (Fig. S3 and S7) and MS spectra (Fig. S5 and S9) are further proof the quantitative preparation of both DOPO-ETES and DOPO-AmdPTES.

The chemical structure of the flame retardants DOPO-ETES and DOPO-AmdPTES after sol–gel process was examined using ^{1}H-NMR and ^{31}P-NMR and FTIR techniques. Specifically, the signal peak observed in the ^{31}P-NMR spectra for both FRs with a chemical shift from δ = 14.59 ppm of pure DOPO to δ = 39.66 ppm for DOPO-ETES and δ = 12.11 ppm for DOPO-AmdPTES confirms the stability of both compounds after sol–gel process (Fig. 1A).

The chemical structure of the final products after sol–gel was also verified by FTIR spectroscopy, as shown in Fig. 1C. The absence of peak around 2385 cm^{-1} that correspond to the stretching vibration of P–H bond (Vasiljević et al. 2015) confirms the successful addition reaction occurred between DOPO and VTES or ICPTES. In addition, the N=C=O absorption band around 2270 cm^{-1} has also been vanished (Hu et al. 2011). The broad band in the range of 3200–3600 cm^{-1} for both FRs is ascribed to the OH stretching of Si–OH. The characteristic peak at 1195 cm^{-1} can be attributed to the stretching vibrations of P=O. The peaks at both 910 and 891 cm^{-1} for DOPO-ETES and DOPO-AmdPTES, respectively, correspond to the stretching vibrations of P–O–Ph, and the absorption band at 1595 cm^{-1} for DOPO-ETES and at 1535 cm^{-1} for DOPO-AmdPTES is related to the existence of P–Ph bonds. The vibrations peak at 750 cm^{-1} belongs to aromatic hydrogen. The bands at 2924 and 3066 cm^{-1} are attributed to C–H stretching vibrations in the aliphatic hydrocarbons. The peak at 1659 cm^{-1} assigns to the H–N absorption of DOPO-AmdPTES, while the band at 1715 cm^{-1} corresponds to C=O stretching. Moreover, the absorption peak within the range of 1039–1095 cm^{-1} can be attributed to the asymmetric stretching of the Si–O–Si and Si–O–C, which confirms the formation of silica network upon the sol–gel reaction.

The silica nanoparticles resulted from sol–gel process (Fig. 1B) of both FRs was evaluated using dynamic light scattering (DLS) as shown in Fig. 1D. DOPO-ETES nanoparticles reveal an average hydrodynamic diameter of 331 nm after 72 h, while the average size of the DOPO-AmdPTES nanoparticles at the same time is around 366 nm. This difference can be attributed to the spacing between DOPO and silane moieties of DOPO-AmdPTES which leads to less hindrance or more flexibility during condensation reaction resulting in higher degree of polymerization. At the same time, the presence of amide groups may form a bigger hydration shell during the DLS measurement. The TGA and differential thermogravimetry (DTG) curves of the nanoparticles measured under the nitrogen atmosphere are shown in Fig. 1E. DOPO-ETES possesses an initial decomposition temperature ($T_{5\%}$, the temperature at 5% weight loss) of 276 °C, whereas DOPO-AmdPTES exhibits a $T_{5\%}$ of 258 °C. Compared to DOPO, which exhibits a $T_{5\%}$ around 220 °C (Xie et al. 2020), both FRs show a higher $T_{5\%}$. However, DOPO-ETES possesses a higher thermal stability compared with DOPO-AmdPTES under a N_2 atmosphere, which is also confirmed by the DSC measurement (Fig. 1F). This difference in the thermal degradation of both FRs can be attributed to the different bond energies of P–C (for DOPO-ETES) and –P–CO–NH (for DOPO-AmdPTES). The char yield (at 800 °C) of DOPO-ETES (42%) is higher than that of DOPO-AmdPTES (35%), which is associated with their molar mass and hence the Si content.

Surface characterization of coated cotton

The nanosol coating of the flame retardants on the cotton substrate was carried out using pad-dry-cure method at different nanosol concentrations. Since the condensation reaction of the silanol groups is not fully completed in solution, it is driven to completion after coating, between the nanosol particles or between the silanol groups and cotton, at a curing temperature of 130 °C yielding a siloxane polymer network on cotton.

Scanning electron microscopy was carried out to observe the surface morphologies of control and coated fabric with an add-on value of ~27 wt% (Fig. 2). The control fabric shows a smooth surface compared to the treated samples. Unlike the sample coated with DOPO-AmdPTES, treated cotton with DOPO-ETES lead to morphological changes in the surface, where a thick layer was observed. Meanwhile, the cross-sectional images reveal a compact

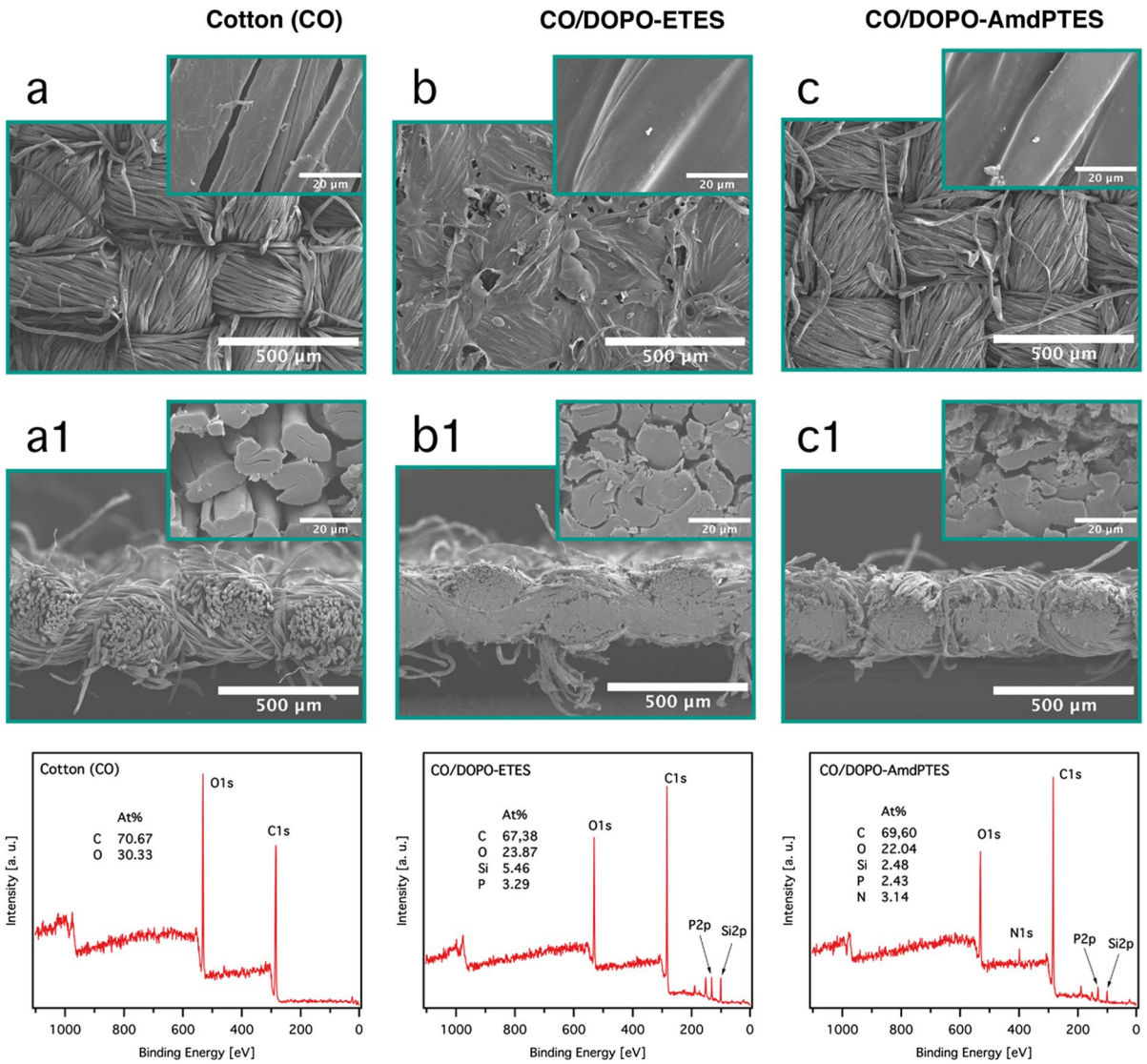

Fig. 2 Scanning electron microscopy (SEM) top view (**a**–**c**) and cross sectional (**a1**–**c1**) images of cotton samples before and after nanosol coating. (below) X-ray photoelectron spectroscopy (XPS) survey spectra of pristine and coated cotton with the elemental compositions of the surface

structure of the fibers indicating a deep finishing of the FRs. The X-ray photoelectron spectroscopy was operated to verify the chemical composition originated from the coating (Fig. 2). Compared with the pure cotton, Si and P elements are detected for both FRs and additionally N element for DOPO-AmdPTES. The chemical composition is summarized in XPS figures, with 5.46% Si and 3.29% P appearing in the surface of cotton coated with DOPO-ETES sols and 2.48% Si and 3.14% P for the surface with DOPO-AmdPTES.

Thermal decomposition behavior

Pristine and coated cotton samples were evaluated with thermogravimetric analysis (TGA) in a nitrogen and air atmosphere with an add-on value of ~27 wt%, as illustrated in Fig. 3. The onset degradation Temperature ($T_{5\%}$), the maximum degradation

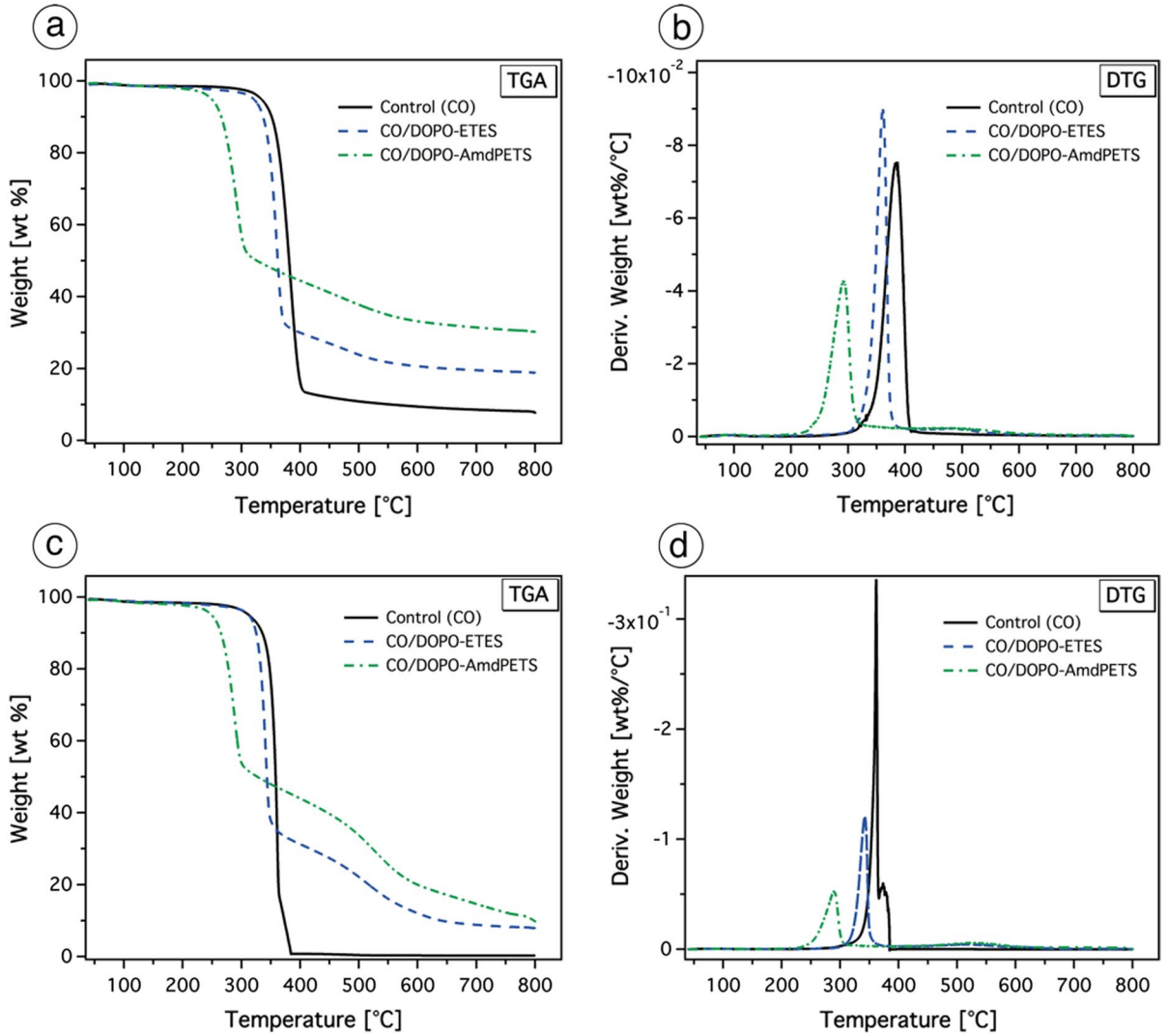

Fig. 3 Thermogravimetric analysis (TGA) and the corresponding differential (DTG) curves of pristine and coated cotton samples measured under nitrogen (**a**, **b**) and air (**c**, **d**) atmosphere at a heating rate of 20 K/min

Table 1 Thermogravimetric analysis (TGA) data of pristine and coated cotton under nitrogen and air atmosphere

	Under nitrogen			Under air		
	$T_{5\%}$ (°C)	T_{max} (°C)	Residue (wt%) at 800 °C	$T_{5\%}$ (°C)	T_{max} (°C)	Residue (wt%) at 800 °C
Cotton (CO)	333.4	384.3	7.4	312.1	361.5 373.2	0.3
CO/DOPO-ETES	320.4	360.5	18.8	312.1	341.3 518.7	7.8
CO/DOPO-AmdPTE	248.9	292.2	30.1	249.2	287.7 531.1	9.5

rate temperature (T_{max}) and the char residue at 800 °C are listed in Table 1. The main thermal decomposition of uncoated cotton under nitrogen atmosphere was observed in the temperature range of 300–420 °C due to the trans-glycosylation of cellulose resulting in aliphatic char and volatiles (Shen and Gu 2009). An additional thermal decomposition stage was observed under air atmosphere for pristine cotton and the residual char rate (0.3%) was lower compared with the nitrogen atmosphere (7.4%) indicating a complete thermo-oxidative degradation of cotton. Compared to pristine cotton, the application of nanosol coatings result in a decrease of both $T_{5\%}$ and T_{max}, which serves to form a protective layer acting as a barrier to mass/heat transfer. However, the sample coated with DOPO-AmdPTES possesses much lower $T_{5\%}$ than that of DOPO-ETES under both nitrogen and air atmospheres for the same add-on value, although the XPS data showed higher content of P and Si elements for the cotton treated with DOPO-ETES nanosols. This observation can be attributed to the catalytic effect between cotton fiber and DOPO-AmdPTES resulted from the worse thermal stability of (P–CO–NH) bonds compared to ($P–CH_2$) bonds of DOPO-ETES as the thermal decomposition of the FRs (see Fig. 1E) exhibit a significant variation in $T_{5\%}$ and T_{max}, which confirms our previous assumption. However, the $T_{5\%}$ and Tmax of cotton treated with DOPO-AmdPTES are in the same range of those obtained from cotton treated with polyphosphate-based flame retardants reported in the literature (Jimenez et al. 2016). This early or fast thermal decomposition allows the P to catalyze the pyrolysis of cellulose and thus promote char formation. Indeed, the residual char rate of treated cotton fabrics with DOPO-AmdPTES nanosols at 800 °C is higher than that of DOPO-ETES under air atmosphere and this difference becomes more noticeable under nitrogen atmosphere (see Table 1). It should also be noted that the cotton fabric treated with DOPO-AmdPTES nanosols undergoes a similar thermal decomposition behavior under air and N_2 atmosphere in the temperature range of 300–420 °C, unlike the cotton treated with DOPO-ETES. For instance, the $T_{5\%}$ of CO/DOPO-AmdPTES was 248.9 °C and 249.2 °C under N_2 and air atmosphere, respectively. While the $T_{5\%}$ of CO/DOPO-ETES reduced by 8 °C under the air atmosphere. Similar behavior was also observed for T_{max1} of both FRs. The abovementioned results indicate that

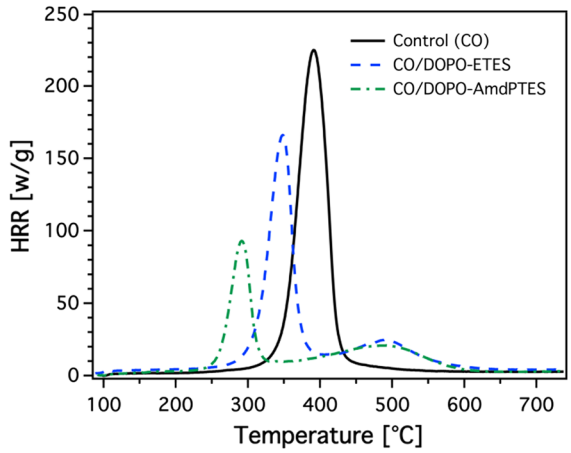

Fig. 4 Microscale combustion calorimetry (MCC) curves of pristine and coated fabrics

the treated cotton with DOPO-AmdPTES nanosols has a better flame-retardant effect than that treated with DOPO-ETES. It is presumed that the mechanism of thermal degradation is strongly correlated with the bonding nature of DOPO subunit as well as the formation of the physical barrier (charring and SiO_2) that prevent mass, heat and flammable transfer gases.

Microscale combustion calorimeter (MCC) (Xu et al. 2022) was used to fully characterize the combustion behavior of cotton fabrics. Figure 4 shows the heat release rate (HRR) curves of pristine and treated cotton. The corresponding combustion data were also presented in Table 2.

The peak HRR (PHRR) value of cotton fabrics decreases by 30.4% and 61.7% after treating with DOPO-ETES and DOPO-AmdPTES nanosols, respectively. Similar results were also observed for the heat release capacity (HRC) and total heat release (THR). As shown in Table 2, the THR of cotton fabric treated with DOPO-ETES is 8.9 kJ/g and 2.8 kJ/g for the sample coated with DOPO-AmdPTES, which are lower than that of pristine cotton 10.6 kJ/g. In a similar manner to TGA results, a significant difference in the pyrolysis behavior between the flame retardants was observed. The cotton treated with DOPO-AmdPTES has lower PHRR, HRC and THR values than cotton treated with DOPO-ETES. Moreover, the temperature at peak HRR (TPHRR) is also much lower, which is consistent with the TGA results. As we stated above, this behavior is ascribed

Table 2 Microscale combustion calorimetry (MCC) results

	HRC J/gK	THR KJ/g	PHRR W/g	T_{PHRR} °C	Residue %
Cotton (CO)	222.1 ± 1.4	10.6 ± 0.3	222.1 ± 1.5	388.1 ± 0.4	8.9 ± 0.8
CO/DOPO-ETES	171.8 ± 2.9	8.90 ± 0.1	154.6 ± 1.2	344.8 ± 0.5	25.5 ± 1.3
			17.20 ± 1.7	441.8 ± 2.5	
CO/DOPO-AmdPTE	102.0 ± 0.2	2.80 ± 0.1	85.00 ± 2.7	288.0 ± 0.6	36.9 ± 0.9
			17.00 ± 0.2	449.6 ± 1.3	

to the faster decomposition of coated fabric with DOPO-AmdPTES which improves the char yield and thus inhibiting the release of combustible volatiles. Table 2 demonstrates that about 26% and 37% of residue can be maintained after MCC test of cotton treated with DOPO-ETES and DOPO-AmdPTES,

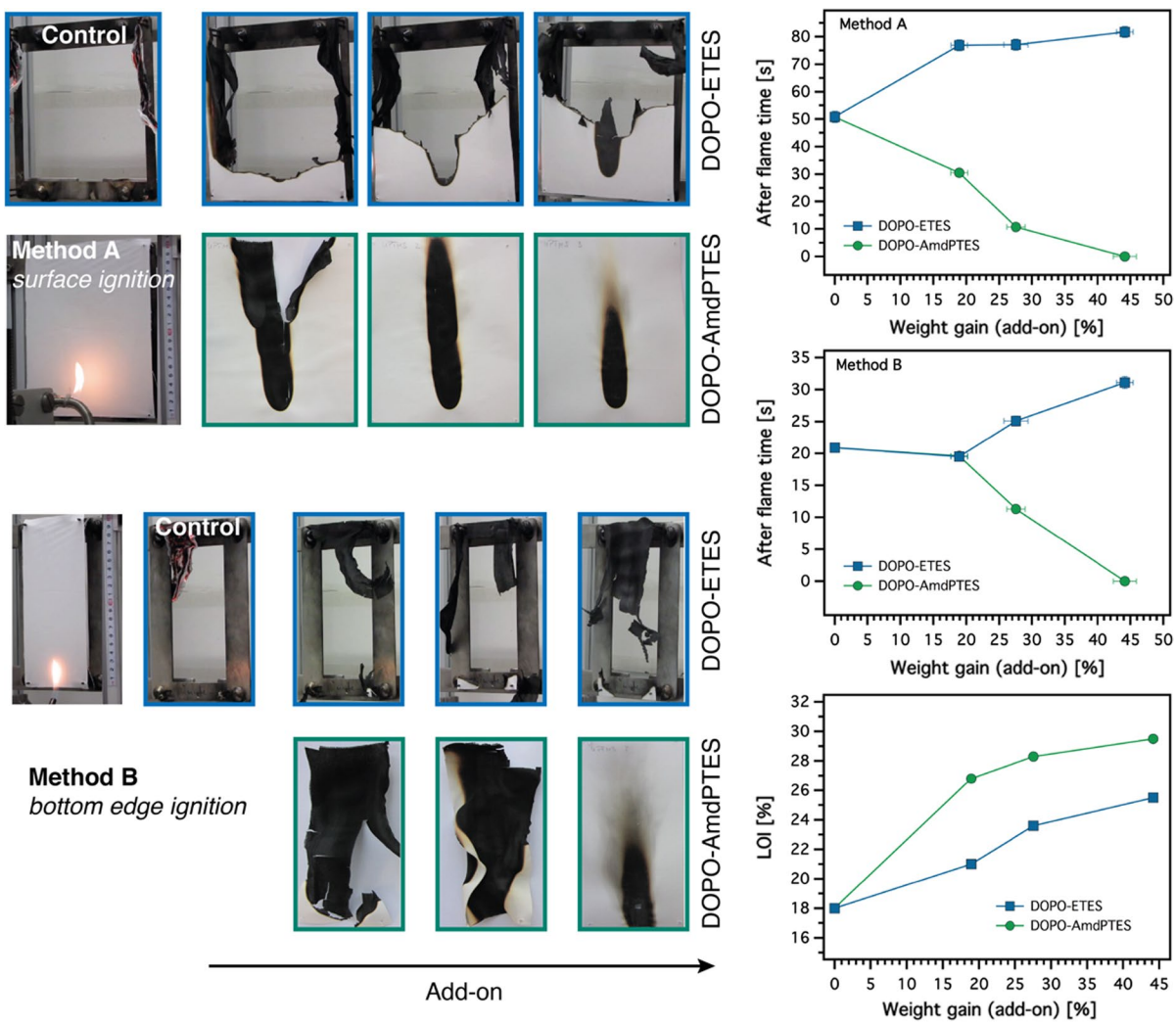

Fig. 5 Digital photographs of untreated and treated cotton fabrics after flame test with surface and bottom edge ignition according to EN ISO 15025 (left). After-flame time and LOI plotted as a function of the add-on value (right)

respectively, indicating the preponderance of condensed phase reaction mechanism of fire resistance. It should be noted that an additional peak appears with a PHRR of 17 W/g and TPHRR above 445 °C for both coated samples. This could be attributed to the pyrolysis of polysiloxane at high temperature.

In sum, the significant reduction of the thermal decomposition indexes for CO/DOPO-AmdPTES compared to CO/DOPO-ETES, were mainly due to the charring process caused by early decomposition of flame retardants that catalyzed the dehydration of cellulose, and at the same time boosting the formation of a silicon-rich barriers to reduce heat release and lower the flammability in the gas phase.

Flame retardancy

In addition to the LOI test, the flame retardancy of textiles was evaluated using a standardized flame test according to EN ISO 15025 with surface and edge ignition methods. The criteria for passing the flame test for both methods are the after-flame time to be less than 2 s and no dripping or hole formation after exposing to a 10 s flame. Figure 5 displays digital images of the untreated and treated cotton samples after the burning test at different add-on values and the after-flame time of both ignition methods and the LOI values were also illustrated as a function of weight gain. The untreated cotton was ignited and fully consumed during both surface and edge flame tests. The treated cotton samples with DOPO-ETES were ignited after flame application with an increase of the after-flame time as the weight gain increases. The flame of the surface ignition test spreads only to the upper edge with a decrease in the igniting area as the add-on value increased. While the burning tests with bottom edge ignition result only in char residual increased at greater weight gain. The increment of after-flame time with edge ignition is less than that of surface ignition test indicating a higher burning growth rate. In contrast, the flame resistance of cotton treated with DOPO-AmdPTES is significantly improved with self-extinguishing behavior (after-flame time less than 2 s and no hole formation) at a weight gain higher than 27% for both ignition methods (see also videos in supplementary information). The after-flame time is decreased with an increase of the content of DOPO-AmdPTES resulting in a low char length. It should be noted that the cotton samples treated with both flame retardants did not exhibit after-glow time upon flame burning tests, unlike the untreated cotton which has an after-glow time of 34.1 s and 28.3 s for surface and bottom edge ignition methods, respectively. The LOI values of treated cotton fabrics increases with the increase of the add-on values of both FRs (see Fig. 5). Samples treated with DOPO-AmdPTES show a higher LOI values compared to those treated with DOPO-ETES at the same weight gain. For instance, the LOI value at a weight gain of 27% was 23% for cotton finished with DOPO-ETES and around 28% for cotton treated with DOPO-AmdPTES.

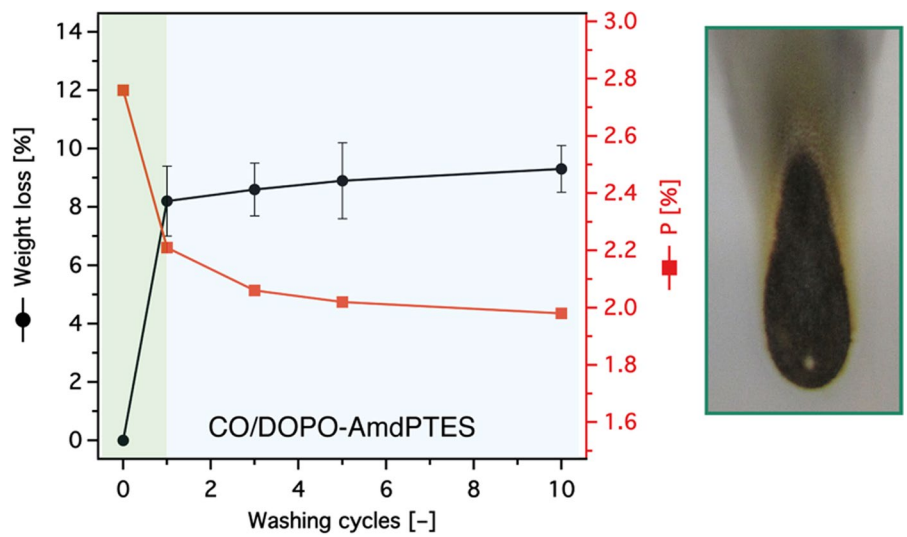

Fig. 6 Weight loss and phosphorus-content of cotton finished with DOPO-AmdPTES after different washing cycles according to ISO 105-C08:2010 (left). Digital photographs of cotton fabrics treated with DOPO-AmdPTES and washed 10 times after flame test with surface ignition method according to EN ISO 15025 (right)

The washing durability of the best performance flame retardants (DOPO-AmdPTES with an add-on value of 35% and LOI value of 28.5%) was evaluated by measuring the change in weight gain (weight loss %) and P-content (%, obtained by ICP-OES) after 1, 3, 5 and 10 washing cycles using a linitester machine according to ISO 105-C06 standard. As shown in Fig. 6, the influence of the washing cycles on the add-on value and hence the P-content can be separated into two regimes. In the first regime (after one washing cycle), the coated cotton displays the greater weight loss of about 8% with a decrease of the phosphorus mass fraction from 2.8% to 2.2%. In contrast, the phosphorus content is slightly decreased in the second regime which associated with the slight increase of the weight loss after ten washing cycles. The LOI value of cotton fabric after 10 laundering cycles was slightly decreased to 27.2%. The flame retardancy of the washed sample was also evaluated using surface ignition method (Fig. 6). The treated cotton with DOPO-AmdPTES exhibits self-extinguishing behavior after 10 washing cycles indicating a semi-durable flame-retardant finishing. In addition to the hydrophobicity nature of DOPO and silane

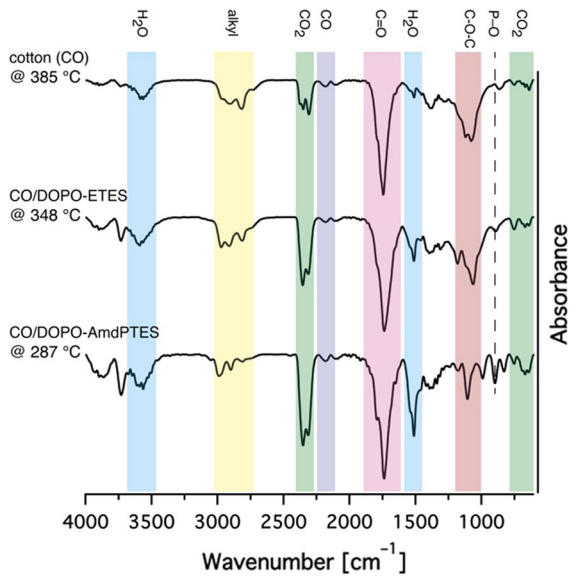

Fig. 8 FTIR spectra of gaseous pyrolysis products extracted from absorbance maxima

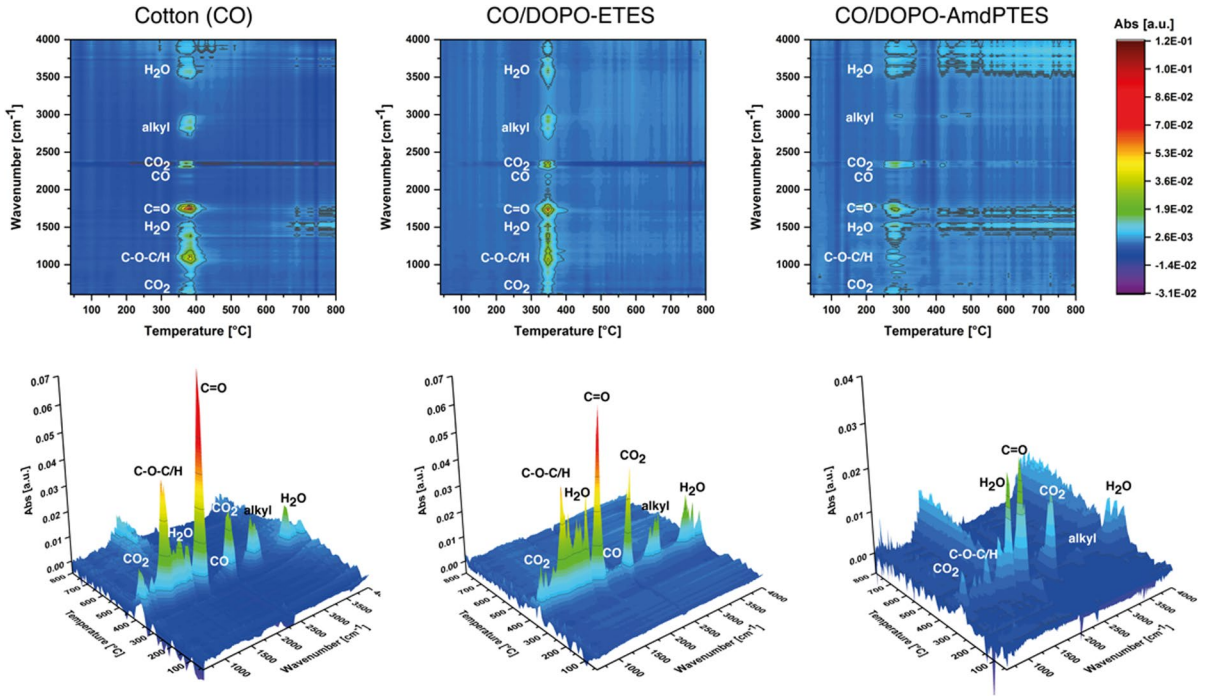

Fig. 7 2D mappings and corresponding 3D diagrams of the pyrolysis volatiles obtained from TG-FTIR analysis

moieties, the durability of the DOPO-AmdPTES flame retardant can be also attributed to the covalent bonds formed between the free silanol groups of the flame retardant and cotton fiber during the thermal curing step, as well as the possible hydrogen-bonding of amido linkages or between the amide units and cellulose.

Gas phase analyses

Thermogravimetric analyzer coupled with a Fourier-transform infrared spectrometer (TG-FTIR)

The gaseous pyrolysis products of the pristine cotton and cotton treated with both DOPO-ETES and DOPO-AmdPTES were evaluated by TGA-IR tests. Figure 7 displays the three-dimensional diagrams and the corresponding two-dimensional mappings of the pyrolysis volatiles produced during the thermal degradation of the samples under a nitrogen atmosphere. The TGA-IR spectra at absorbance maxima are shown in Fig. 8.

The peak signal at maxima of both flame retardants is shifted to lower time/temperature compare with the spectrum of control cotton, which is ascribed to the earlier depolymerization and dehydration of cellulose induced by acid catalyst. Obviously, the absorbance maxima of cotton treated with DOPO-AmdPTES appears at a lower temperature (287 °C) than that treated with DOPO-ETES (348 °C). Typical thermal degradation products of the pristine cotton can be classified as nonflammable gases including gaseous water (3450–3700 cm^{-1}) and CO_2 with stretching and binding vibrations around 2357 and 575 cm^{-1}, respectively. While, peaks at 2630–3030 cm^{-1}, 2183 cm^{-1}, 1600–1875 cm^{-1} and 1068 cm^{-1} correspond to combustible volatiles of hydrocarbons (–CH_2, –CH_3), carbon monoxide, carbonyls (C=O) and ethers (C–O–C), respectively.

Compared with the pristine cotton, a new weak peak can be observed at 898 cm^{-1} in the spectra after decomposition for treated cotton assigned to P–O stretching, revealing that the DOPO-based flame retardants may also exhibit a gas phase mechanism in addition to the condensed-phase action. Figure 7

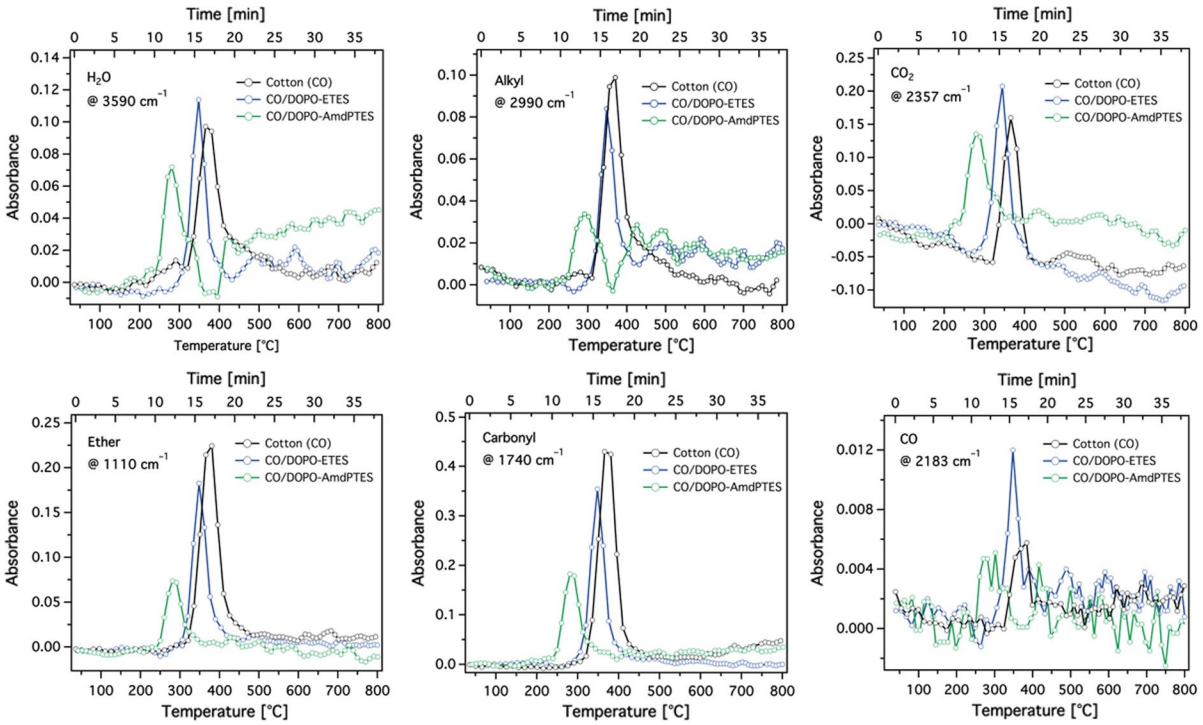

Fig. 9 Absorption intensities at a specified wavenumber of typical gaseous volatiles during thermal degradation (obtained from TGA-FTIR tests) of pristine and treated cotton

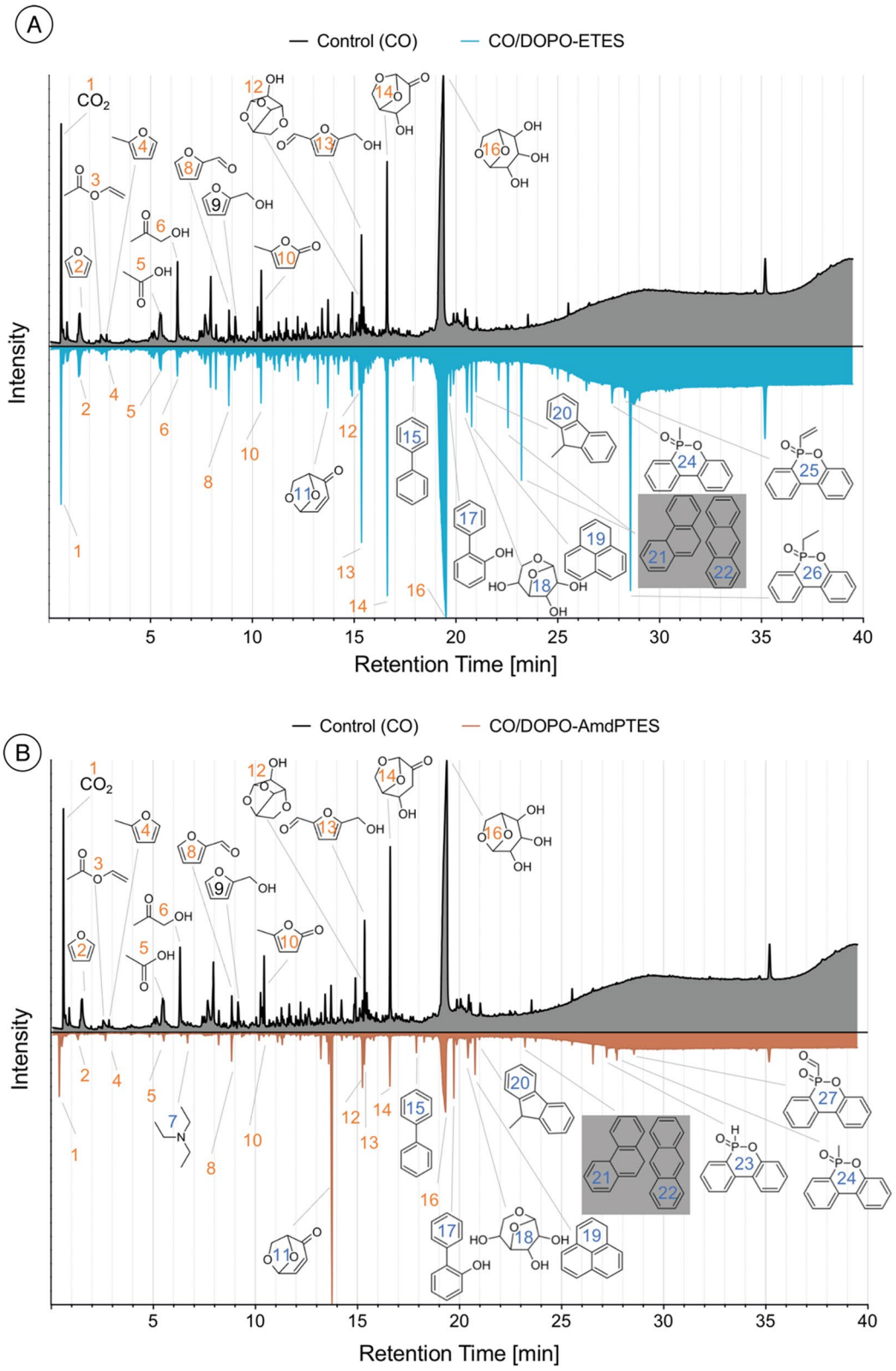
A
Control (CO)
CO/DOPO-ETES
Intensity
Retention Time [min]
B
Control (CO)
CO/DOPO-AmdPTES
Intensity
Retention Time [min]

◂**Fig. 10** Total ion chromatogram (TIC) obtained by pyrolysis gas chromatography mass spectrometry (Py-GC/MS) of untreated and treated cotton fabric with DOPO-ETES (**A**) and DOPO-AmdPTES (**B**) at 700 °C

clearly indicates that the peak absorption intensities of flammable and nonflammable gases at maxima for cotton treated with DOPO-AmdPTES are weaker than those for the pristine cotton and cotton treated with DOPO-ETES.

For further investigation, the intensity of pyrolysis products at a specified wavenumber was also analyzed as a function of both time and temperature (Fig. 9) to determine the influence of the DOPO based flame retardants on the pyrolysis volatiles of cotton. Unlike the cotton treated with DOPO-ETES, the decomposition time and hence the pyrolysis temperature of treated cotton with DOPO-AmdPTES are reduced by at least 10 min and approximately 100 °C. The peak intensity of volatiles, in absorption FTIR spectroscopy, is proportional to its concentration according to Beer-Lambert law. Thus, the significant reduction of peak absorption intensities of combustible gases during the degradation of cotton treated with DOPO-AmdPTES is due to the lowered amounts of released flammable volatiles, revealing that DOPO-AmdPTES nanosols restrains the cellulose decomposition. For instance, the peak intensities of carbonyls and alkyls are reduced by about 60%, while that of ethers is lower by 75% relative to pristine cotton. Moreover, the liberation of nonflammable volatiles (H_2O and CO_2) can be observed over the whole degradation time, which is clearly indicative of dehydration and decarboxylation of cellulose promoting the char-formation. In contrast, the peak intensities of the flammable volatiles of cotton treated with DOPO-ETES is not significantly reduced compared to uncoated cotton indicating an entire combustion of cellulose. It is worth noting that the signal of hydrocarbons for the treated cottons show an additional absorption peak start at 14 min (360 °C) which can be attributed to the decomposition of flame retardants during the formation of SiO_2 and graphitic char.

Unlike DOPO-ETES, the TGA-FTIR analysis indicates that DOPO-AmdPTES effectively improves the fire resistance of cellulose by inhibiting the formation of combustible volatiles along with the release of nonflammable gases that dilute the density of pyrolysis products in the gaseous phase. In addition to the physical effect mode of action, the detection of phosphorous-containing compounds in the gas phase may also indicate their chemical contribution of extinguishing the flame by reducing the concentration of free radicals. At the same time, the early decomposition of DOPO-AmdPTES flame retardant also facilitates and promotes the char-formation of cellulose in the condensed phase.

Pyrolysis–gas chromatography-mass spectrometry (Py-GS/MS)

Pristine cotton undergoes a thermal degradation through an intermediate state called activated cellulose (Arseneau 1971), where the degree of polymerization decreases without mass loss. The further decomposition of this activated cellulose involves two competitive mechanisms, namely dehydration and depolymerization (Tsuge et al. 2011; Kawamoto 2016).

In order to investigate the main pyrolysis volatile products resulting from untreated and treated cotton in the pyrolysis process, pyrolysis gas chromatography and mass spectrometry (Py-GC/MS) analyses were conducted at 700 °C for 1 min. The total ion chromatograms (TIC) demonstrating the peaks of different retention times are shown in Fig. 10. The mass spectra fragmentation pattern of the peaks was identified using three different databases (NIST Standard Reference Database Number 69, MassBank and SpectraBase) and the major characteristic compounds with their relative percentage are summarized in Table S1.

The degradation via dehydration leads to the formation of anhydrocellulose and aromatic char with a consecutive release of water and small molecule gases. In depolymerization, the degradation reaction originates from the heterolytic cleavage of acetal bonds of the glycosidic units to form levoglucosan (LGA, 16) as an intermediate of pyrolysis products. Levoglucosan exhibits further decomposition steps rereleasing several flammable fragments and tar including compounds, such as aldehydes, ketones, acids, ethers, furans and furfural (Fig. 11) (Shen and Gu 2009; Shafizadeh 1968). Therefore, reducing the production of LGA inhibits the formation pathway towards combustible substances.

Unlike CO/DOPO-ETES sample, the peak numbers of cotton treated with DOPO-AmdPTES were

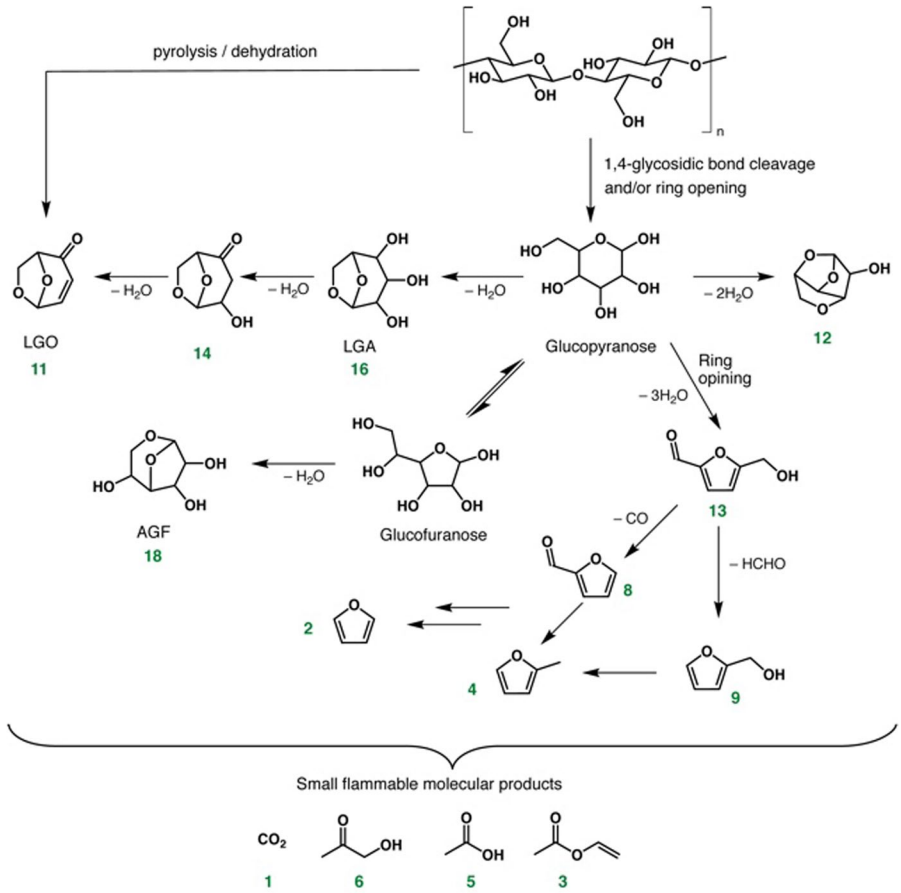

Fig. 11 Proposed pathways of cellulosic pyrolysis with compounds detected by pyrolysis gas chromatography mass spectrometry (Py-GC/MS) measurements

dramatically reduced and the percentage areas of volatile products were significantly decreased along with the release of nonflammable small molecules. The peak of the intermediate compound (LGA **16**) that appeared at about 19.3 min was reduced by 32% for CO/DOPO-AmdPTES compared to control cotton, while the relative percentage of LGA produced from the pyrolysis of CO/DOPO-ETES was increased by 13%. The pyrolysis of DOPO-finished cotton produced new degradation products including levoglucosenone (LGO **11**), aromatic compounds (**15**, **17**, **19**, **20**, **21**, **22**) as well as DOPO (**23**) and DOPO derivatives (**24**, **25**, **26**, **27**), which reveals the change of the degradation pathways. In particular, LGO, with 20% yield, displays the highest intensity peak within the TIC spectrum of CO/DOPO-AmdPTES. LGO can either be generated in direct pathway from the polymer chain of cellulose via pyrolysis/dehydration process, or through indirect pathway by a dehydration process of anhydrosugars, such as LGA and 1,6-anhydro-*β*-D-glucofuranose (AGF **18**) in the gas phase (Fig. 11) (Kandola et al. 1996). However, the high yield of LGO production indicates a phosphor-based catalytic dehydration of CO/DOPO-AmdPTES (Kudo et al. 2021), which promote the formation of an inert char protecting the textile from further degradation.

Besides, the new observed peaks including biphenyl (**15**), o-hydroxybiphenyl (**17**) and the rearranged aromatic compounds (**19**, **20**, **21** and **22**) are mainly attributed to the decomposition products of DOPO derivatives, which results in the liberation of POx moieties that either initiate and enhance the char formation of cotton in the condensed phase or behave as radical scavenger in the gas phase delaying the decomposition process. DOPO (**23**) and its derivatives (**24**, **25**, **26** and **27**) were also detected as pyrolysis products and even though a Δm of 47 u (PO splitting-off) was detected in all DOPO mass spectra, a contribution of PO-radicals in the gas phase during

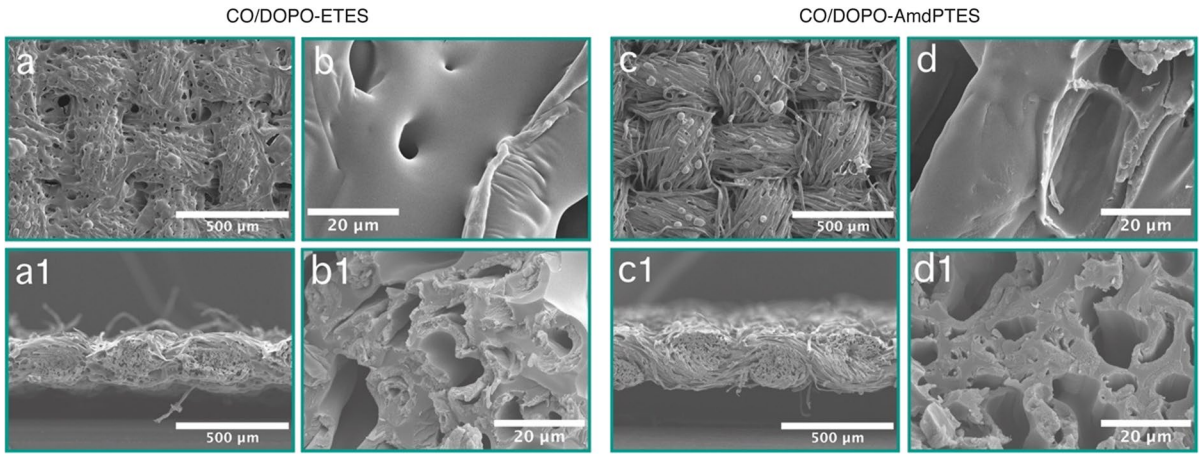

Fig. 12 SEM top view and cross-sectional images of burned cotton samples finished with DOPO-ETES (**a**, **a1**, **b**, **b1**) and DOPO-AmdPTES (**c**, **c1**, **d**, **d1**) at two different scale bars (500 and 20 µ)

pyrolysis cannot be proven using Py-GC/MS. Drawing conclusions from fragmentation reactions by electron ionization about pyrolysis fragmentation is complex and needs further investigations (Moldoveanu 1998). However, the low relative area percentages of DOPO derivatives and their pyrolysis products indicate the domination of the condensed phase activity of the flame retardants, which is nicely supported by the char analysis in the next subsection.

Condensed phase analyses

Scanning electron microscopy (SEM)

Scanning electron microscopy images of the char residues for treated cotton are obtained after being subjected to the surface ignition test. The untreated fabric was completely consumed during burning without residual char. As observed in Fig. 12, the surface of the fabrics finished with DOPO-ETES shows a dense morphology indicating that the sample undergoes a combustion reaction with oxygen and flammable gas. It should be noted that the after-burn residues of CO/DOPO-ETES maintains an intact char skeleton to some extent, although the sample cannot pass the burning test. The structure of the cotton fabric treated with DOPO-AmdPTES retains its skeleton completely and forms compact char layer along with scattered bubbles appear on the surface of fabric as a result from the escape of volatile and non-volatile gases during combustion process. This observed morphology suggests an intumescent action of DOPO-AmdPTES flame retardant, which prevents the mass and heat transfer between the burning material and the flame zone resulting in self-extinguishing behavior. However, no morphological difference was observed for the cross-sectional images of both flame retardants except that the thickness of the cotton sample treated with DOPO-ETES after burning is less than that of CO/DOPO-AmdPTES which may be related to the degradation of the fabric.

XPS analysis of charred textile samples

XPS analysis was further performed on the char residues of treated cotton samples in order to explore the elemental composition and the form of chemical bonds and their corresponding results are demonstrated in Fig. 13. The char residues of treated cotton are comprised of carbon, oxygen, phosphorus and silicon elements. Char residues of the fabric coated with DOPO-AmdPTES exhibits an additional peak assigned to nitrogen element. However, the presence of phosphorous in the char residues confirms the validity of the condensed phase activity of DOPO derivatives via phosphorylation during the flame-retardants decomposition. The results of the elemental composition show a higher carbon content of CO/DOPO-AmdPTES residues than that of CO/DOPO-ETES indicating its improvement of charring ability, which is consistent with the results obtained from the TGA measurement. In contrast, the P and Si

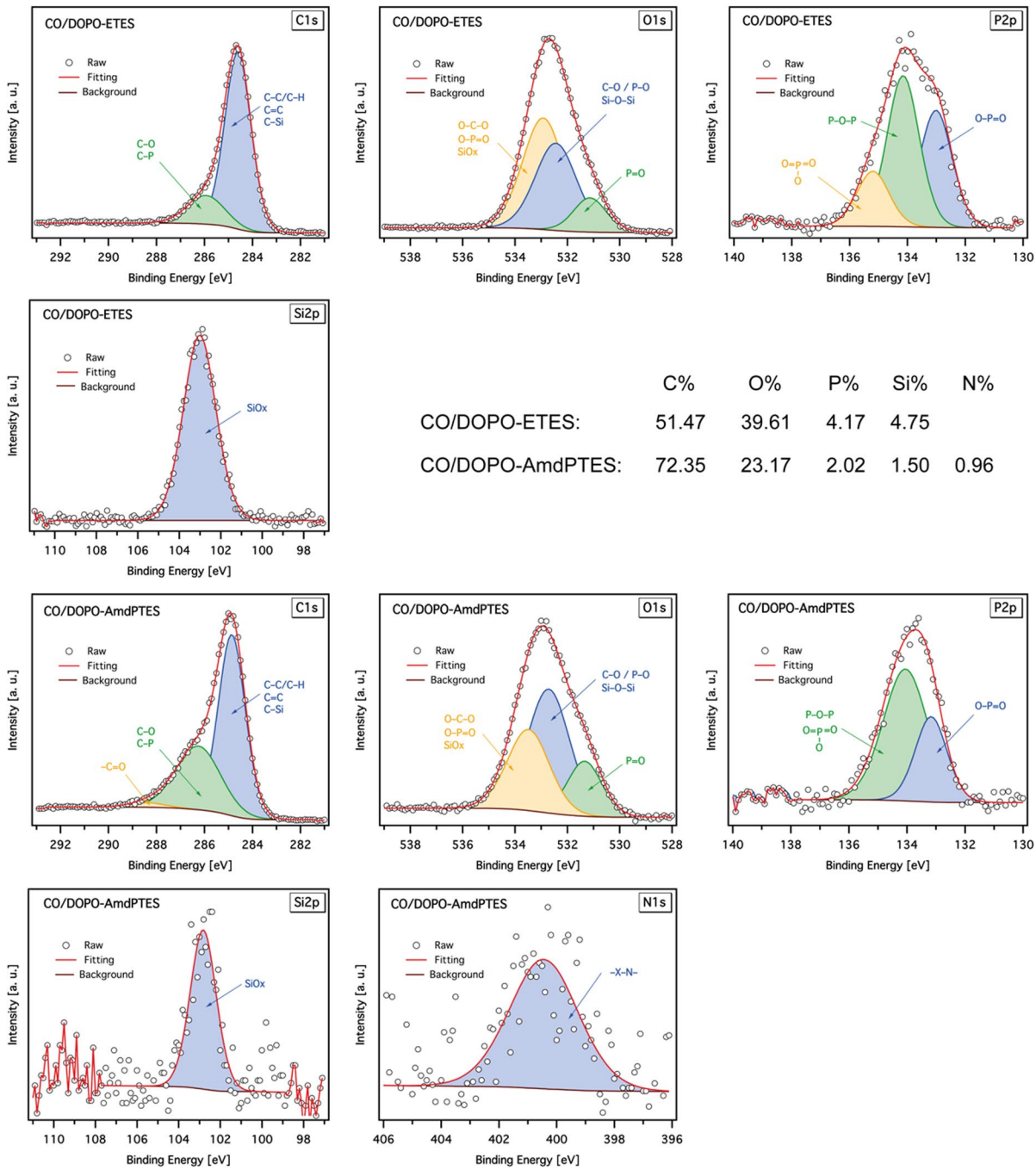

Fig. 13 High resolution XPS spectra of the char residues of treated cotton with flame retardants after burning test

content of CO/DOPO-ETES residues is much higher, although the sample did not pass the burning test. These observations can be explained, as mentioned before, due to the stability of DOPO-ETES towards the thermal degradation which delays its activity as flame retardant via acid catalyzed dehydration resulting in less charring and more flammable volatiles and hence complete combustion of cellulose.

The deconvoluted C1s spectrum of cotton treated with DOPO-ETES shows two characteristic peaks

at 284.6 eV assigned mainly to both C–C and C=C, while the peak at 286 eV corresponds to C–O, C–N and C–P linkages. For the residues of treated cotton with DOPO-AmdPTES, the additional weak peak centered at a binding energy of 288.4 eV should be ascribed to C=O, which may correspond to the structure of the flame retardant or to dehydrated units of cellulose. The high resolution O1s spectra consist of three peaks corresponding to double-bonded oxygen in P=O groups and C=O groups (only for CO/DOPO-AmdPTES residues) at a binding energy of 531.2 eV and a single-bonded oxygen in C–P–O, C–O–C and Si–O–Si at around 532.6 eV. The third peak of O1s spectra, with a binding energy around 533 eV (for CO/DOPO-ETES) and 533.5 eV (CO/DOPO-AmdPTES), are the contribution of both double- and single-bonded oxygen in O–C–O, O–P=O as well as SiOx of silica char. The deconvoluted P2p region spectrum of CO/DOPO-AmdPTES shows two peaks at 133.2 eV assigned to O=P–O group formed during the thermal degradation of DOPO, while the signal at 134.1 eV is attributed to the structure of pyrophosphoric acid and metaphosphoric acid in P–O–P and PO_3, respectively. Similar linkages were also observed for the P2p survey of CO/DOPO-ETES char, except that the linkages of P–O–P and PO_3 can be fitted in two different peaks at a binding energy of 134.2 and 135.2 eV. The char formation of silica for both flame retardants was also confirmed through the Si2p spectra, which both show a binding energy around 103 eV representing the Si–O–X groups (where X = Si, P or C). In addition, the 0.96 at.% of N element in the residues of CO/DOPO-AmdPTES, which displays a broad peak in the binding energy rang of 397–404 eV, reveals the presence of nitrogen compounds in the char residues in the form of N–P and N–C linkages as well. So, the abovementioned results indicate that DOPO silanes more likely conduce to the production of phosphorus-based acid catalysts, which act as dehydrating agents towards carbonaceous char formation. Additionally, the carbon char layers are further enhanced by the formation of thermally insulated silicon oxide barriers. The results also indicate the presence of nitrogen in the residual carbon of CO/DOPO-AmdPTES, which enhance the formation of intumescent char as depicted in the SEM images.

Molecular dynamics (MD) simulation & flame-retardant mechanism

In order to get an insight into the thermal degradation of the flame retardants, a molecular dynamics (MD) simulation study was performed using DFTB + simulation package. For simplification, the triethoxysilane moieties were omitted from the structures prior to simulation. Before the MD simulation, the flame-retardant molecules were geometrically optimized to obtain the lowest energy points and the optimized bond lengths. The obtained results are consistent with the crystal structure of DOPO reported in the literature (Schäfer et al. 2007; Weinert and Döring 2021) for which P–C_{Ar} = 1.78–1.79 Å, P–O = 1.62 Å, P=O = 1.54–1.57 Å, P–CH_2 = 1.8 Å,

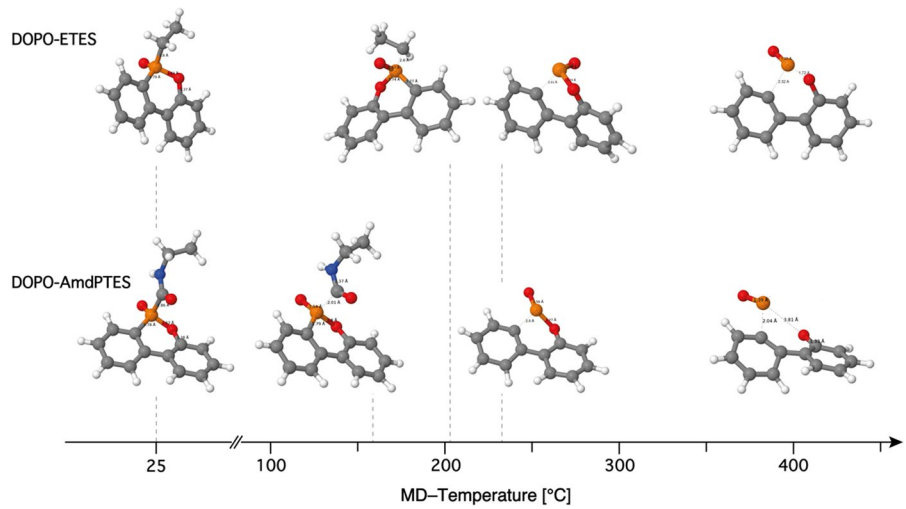

Fig. 14 Schematic representation of the molecular dynamic simulations performed for the studied flame retardants using DFTB + simulation package in the temperature range of 25–450 °C

P–CO = 1.86 Å, C=C = 1.4 Å. The bond angle between carbon atoms in the benzene rings is ranging between 119.1° and 120.4° and the O–P–C_{Ar} bond angle is around 100.3° and 102° for DOPO-ETES and DOPO-AmdPTES, respectively. Figure 14 displays the lowest energy structures of both molecules and their corresponding MD-temperature after MD simulations in the temperature range of 25–450 °C. Our MD simulations clearly indicate that the first bond dissociation originates between the DOPO and alkyl for ETES or amido-carbonyl for AmdPTES as the temperature increases. The bond dissociation energy of P–CO bond for DOPO-AmdPTES was calculated to be around 339 kJ/mol which is lower than that of P–CH_2 for DOPO-ETES (around 427 kJ/mol) at 25 °C. This observation emphasizes that the decomposition of DOPO-AmdPTES flame retardant will begin at a lower temperature compared to DOPO-ETES (see also the simulation videos in supplementary information), which is in line with the experimental results obtained from TGA and MCC. Consecutively, DOPO fragments in both flame retardants undergo further decomposition at higher temperatures where the single bond between the phosphorus and the carbon atom of the aromatic ring are segregated followed by a dissociation of the P–O bond releasing a P=O molecule (Fig. 14). These dissociation pathways are in good agreement with the results observed in Py-GC/MS study. It should be noted that the decomposition temperatures obtained from MD simulation are lower than that of the experimental results which could be attributed to the fact that the simulation was performed for isolated single molecule under steady conditions that differ from the experimental ones.

According to the analysis of the experimental results and based on the study of density functional theory, the possible flame-retardant mechanism of DOPO-ETES and DOPO-AmdPTES are shown in Fig. 15. The flame retardancy of treated cotton is mainly attributed to the flame-retarding effect in condensed phase and much less or negligible activity in the gaseous phases. Due to the early decomposition of the DOPO-AmdPTES flame retardant in comparison to DOPO-ETES, CO/DOPO-ETES exhibited a relatively poor flame retardancy. In the gas phase, the Py-GC/MS as well as TGA-FTIR experiments suggested the release of phosphorous (PO) free radicals into the gas phase from the decomposition of DOPO moieties during the pyrolysis of both flame retardants (Qian et al. 2013, 2012). These radicals behave as scavengers and trap the active H and OH radicals, diluting the gas phase and hence preventing the continuous burning. Meanwhile, less flammable gasses were produced in the case of cotton treated with DOPO-AmdPTES due to the dilution of the gas phase with nonflammable gasses combined with the formation of carbon layer at the early decomposition stage induced by the acid catalyzed dehydration of cellulose. Combined with the early thermal decomposition of DOPO-AmdPTES, the water produced during the cellulose pyrolysis also play a significant role of the phosphate/polyphosphate formation

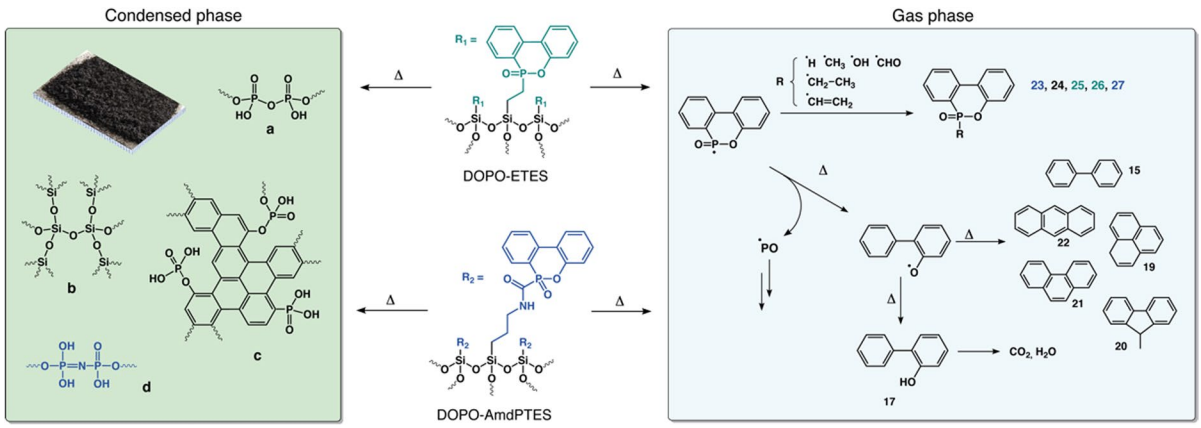

Fig. 15 Structural charts of possible flame-retardant degradation mechanism of DOPO-ETES and DOPO-AmdPTES

after the first and second bonds dissociation of FRs (see Fig. 14) rather than the formation of PO free radicals resulting in high phosphorous contents in the residual char. In the condensed phase, the high char yield obtained from the TGA experiment, supported by high phosphorous contents of the char residues, strongly indicate the formation of dense carbon layers (Fig. 15c) induced by the polyphosphoric acid (Fig. 15a) during the decomposition of phosphorus-containing components (Lewin and Weil 2001). Additionally, the presence of silicon atoms was also beneficial to the enhancement of the char layers by the formation of silicon dioxide networks (Fig. 15b). The detection of nitrogen atoms in the condensed phase of the residual char of CO/DOPO-AmdPTES sample can be rationalized by the presence of phosphorus oxynitride (Fig. 15d) which occurs during the degradation process. The resulting protective layers effectively shielded the substrate from air, heat and mass transmission during cellulose pyrolysis. In conclusion, in contrast to cotton coated with DOPO-ETES, the flame retardancy of coated fabric with DOPO-AmdPTES, has been greatly improved, which is attributed to its earlier onset degradation.

Conclusion

In summary, flame retardants derived from two different silane compounds bearing DOPO were synthesized and coated on the surface of cotton fabrics via sol–gel method in order to investigate their efficiency in fire safety. The morphological structure and the elemental composition of the modified fabric were investigated by SEM and XPS. Flame test with surface and bottom edge ignition method, according to EN ISO 15025, and MCC were applied to evaluate the flame retardancy of the pristine and treated fabrics. Unlike DOPO-ETES, the results showed that the after-flame time decreases as a function of the weight percentage of DOPO-AmdPTES and endows cotton with self-extinguishing behavior. The peak at heat release rate (PHRR), total heat release (THR) and heat release capacity (HRC) of the flame retardants were significantly reduced compared to control sample. The treated cotton with DOPO-AmdPTES showed a semi-durability up to 10 washing cycles maintaining its flame retardancy. In addition, the thermal stability of untreated and treated cotton were investigated by TGA which indicated a reduction in the initial decomposition temperature of CO/DOPO-AmdPTES sample by at least 85 °C compared with CO/DOPO-ETES sample that only underwent a reduction of 13 °C. Meanwhile, the residual char of the treated sample was enhanced for finished samples under both nitrogen and air atmospheres. Moreover, the flame-retardant mechanism was evaluated from both gas and condensed phases via real time Fourier transform infrared spectroscopy (TGA-FTIR), pyrolysis–gas chromatography-mass spectrometry (Py-GC/MS), SEM and XPS, and the experimental results were also supported by a simulation study using density-functional theory (DFT). The results of the abovementioned methods confirmed that the main mechanism of the studied FRs is related to the condensed phase mode of action triggered by acid catalyst, where the decomposition of CO/DOPO-AmdPTES ahead of DOPO-ETES as well as pristine cotton, and hence catalysis of char formation, play the key role for excellent flame retardancy.

Acknowledgments abcr GmbH is gratefully acknowledged for the granting a project-related chemical discount and the donation of flame retardants. The authors would like to thank DTNW Öffentliche Prüfstelle GmbH for the ICP-OES analyses, CHT Germany GmbH for the Py-GC/MS analyses, Dr. Florian Uteschil for the ESI-HRMS measurements, ARCCA at Cardiff for the generous allocation of computational resources. We acknowledge support by the Open Access Publication Fund of the University of Duisburg-Essen.

Author contributions WA, DD OZ and BA wrote the main manuscript text. Conceptualization, methodology WA, and TM-G. Investigation WA, SC, AS, VS, HMP, OZ, LK, RW, YF and BA. Review and editing, supervision, funding acquisition JSG, TT and TM-G. All authors have approved the final version of the manuscript.

Funding Open Access funding enabled and organized by Projekt DEAL. The research project of the research associations Forschungskuratorium Textil (FKT) was supported by the Federal Ministry for Economic Affairs and Climate Action and the AIF (German Federation of Industrial Research Associations e.V.) within the framework of the industrial collective research (IGF) program (IGF No. 19617 N) and by the Federal Ministry for Economic Affairs and Climate Action (BMWK) (ZIM ZF4139703EB9) on the basis of a decision by the German Bundestag.

Data availability Not applicable.

Declarations

Conflict of interest The author(s) declared no potential conflicts of interest with respect to the research, authorship, and/or publication of this article.

Ethics approval and consent to participate Not applicable.

Consent for publication Not applicable.

References

Arseneau DF (1971) Competitive reactions in the thermal decomposition of cellulose. Can J Chem 49(4):632–638. https://doi.org/10.1139/v71-101

Bifulco A, Varganici CD, Rosu L, Mustata F, Rosu D, Gaan S (2022) Recent advances in flame retardant epoxy systems containing non-reactive DOPO based phosphorus additives. Polym Degrad Stab 200:109962. https://doi.org/10.1016/j.polymdegradstab.2022.109962

Chen X, Ye J, Yuan L, Liang G, Gu A (2014) Multi-functional ladder-like polysiloxane: synthesis, characterization and its high performance flame retarding bismaleimide resins with simultaneously improved thermal resistance, dimensional stability and dielectric properties. J Mater Chem A 2(20):7491–7501. https://doi.org/10.1039/C4TA01292E

Chen Y, Liao Y, Zhang G, Zhang F (2022) Durable flame-retardant finishing of cotton with a reactive phosphorus-based environmental flame retardant. J Nat Fibers. https://doi.org/10.1080/15440478.2022.2070327

Chernyy S, Ulah S, Sørensen G, Tordrup SW, Pedersen PB, Almdal K (2015) DOPO-VTS-based coatings in the realm of fire retardants for cotton textile. J Appl Polym Sci 132(19):41955. https://doi.org/10.1002/app.41955

Čolović M, Vasiljević J, Štirn Ž, Korošin NČ, Šobak M, Simončič B, Demšar A, Malucelli G, Jerman I (2021) New sustainable flame retardant DOPO-NH-functionalized polyamide 6 and filament yarn. Chem Eng J 426:130760. https://doi.org/10.1016/j.cej.2021.130760

Feng Y, Li X, Zhao X, Ye Y, Zhou X, Liu H, Liu C, Xie X (2018) Synergetic improvement in thermal conductivity and flame retardancy of epoxy/silver nanowires composites by incorporating "branch-like" flame-retardant functionalized graphene. ACS Appl Mater Interfaces 10(25):21628–21641. https://doi.org/10.1021/acsami.8b05221

Gaus M, Lu X, Elstner M, Cui Q (2014) Parameterization of DFTB3/3OB for sulfur and phosphorus for chemical and biological applications. J Chem Theory Comput 10(4):1518–1537. https://doi.org/10.1021/ct401002w

Gu L, Qiu C, Qiu J, Yao Y, Sakai E, Yang L (2020) Preparation and characterization of DOPO-functionalized MWCNT and its high flame-retardant performance in epoxy nanocomposites. Polymers 12(3):613. https://doi.org/10.3390/polym12030613

Gu J, Yan X, Li J, Qian Y, Zhu C, Qi D (2021) Durable flame-retardant behavior of cotton textile with a water-based ammonium vinyl phosphonate. Polym Degrad Stab 191:109658. https://doi.org/10.1016/j.polymdegradstab.2021.109658

Hourahine B, Aradi B, Blum V, Bonafé F, Buccheri A, Camacho C, Cevallos C, Deshaye M, Dumitrică T, Dominguez A et al (2020) DFTB+, a software package for efficient approximate density functional theory based atomistic simulations. J Chem Phys 152(12):124101. https://doi.org/10.1063/1.5143190

Hu S, Hu Y, Song L, Lu H (2011) Effect of modified organic–inorganic hybrid materials on thermal properties of cotton fabrics. J Therm Anal Calorim 103(2):423–427. https://doi.org/10.1007/s10973-010-1093-1

Jimenez M, Guin T, Bellayer S, Dupretz R, Bourbigot S, Grunlan JC (2016) Microintumescent mechanism of flame-retardant water-based chitosan–ammonium polyphosphate multilayer nanocoating on cotton fabric. J Appl Polym Sci 133(32):43783. https://doi.org/10.1002/app.43783

Kanat M, Eren T (2019) Synthesis of phosphorus-containing flame retardants and investigation of their flame retardant behavior in textile applications. J Appl Polym Sci 136(36):47935. https://doi.org/10.1002/app.47935

Kandola BK, Horrocks A, Price D, Coleman G (1996) Flame-retardant treatments of cellulose and their influence on the mechanism of cellulose pyrolysis. J Macromol Sci Part C Polym Rev 36(4):721–794. https://doi.org/10.1080/15321799608014859

Kawamoto H (2016) Review of reactions and molecular mechanisms in cellulose pyrolysis. Curr Org Chem 20(23):2444–2457. https://doi.org/10.2174/2213337203666160525102910

König A, Kroke E (2012) Flame retardancy working mechanism of methyl-DOPO and MPPP in flexible polyurethane foam. Fire Mater 36(1):1–15. https://doi.org/10.1002/fam.1077

Kudo S, Huang X, Asano S, Ji H (2021) Catalytic strategies for levoglucosenone production by pyrolysis of cellulose and lignocellulosic biomass. Energy Fuels 35(12):9809–9824. https://doi.org/10.1021/acs.energyfuels.1c01062

Kundu CK, Yu B, Gangireddy CSR, Mu X, Wang B, Wang X, Song L, Hu Y (2017) UV grafting of a DOPO-based phosphoramidate monomer onto polyamide 66 fabrics for flame retardant treatment. Ind Eng Chem Res 56(6):1376–1384. https://doi.org/10.1021/acs.iecr.6b04188

Kundu CK, Song L, Hu Y (2020a) Sol-gel coatings from DOPO-alkoxysilanes: Efficacy in fire protection of polyamide 66 textiles. Eur Polym J 125:109483. https://doi.org/10.1016/j.eurpolymj.2020.109483

Kundu CK, Wang X, Rahman MZ, Song L, Hu Y (2020b) Application of chitosan and DOPO derivatives in fire protection of polyamide 66 textiles: towards a combined gas phase and condensed phase activity. Polym Degrad Stab 176:109158. https://doi.org/10.1016/j.polymdegradstab.2020.109158

Lewin M, Weil ED (2001) Mechanisms and modes of action in flame retardancy of polymers. In: Price D (ed) Horrocks A. Fire retardant materials, Woodhead Publishing, pp 31–68

Liang S, Neisius M, Mispreuve H, Naescher R, Gaan S (2012) Flame retardancy and thermal decomposition of flexible polyurethane foams: structural influence of organophosphorus compounds. Polym Degrad Stab 97(11):2428–2440. https://doi.org/10.1016/j.polymdegradstab.2012.07.019

Liu C, Xing T, Wei B, Chen G (2018) Synergistic effects and mechanism of modified silica sol flame retardant systems on silk fabric. Mater 11(10):1842. https://doi.org/10.3390/ma11101842

Lu SY, Hamerton I (2002) Recent developments in the chemistry of halogen-free flame retardant polymers. Prog Polym Sci 27(8):1661–1712. https://doi.org/10.1016/S0079-6700(02)00018-7

Mayer-Gall T, Knittel D, Gutmann JS, Opwis K (2015) Permanent flame retardant finishing of textiles by allyl-functionalized polyphosphazenes. ACS Appl Mater Interfaces 7(18):9349–9363. https://doi.org/10.1021/acsami.5b02141

Moldoveanu SC (1998) Analytical pyrolysis of natural organic polymers. Elsevier

Müller P, Bykov Y, Döring M (2013) New star-shaped phosphorus-containing flame retardants based on acrylates for epoxy resins. Polym Adv Technol 24(9):834–840. https://doi.org/10.1002/pat.3151

Nazir R, Parida D, Borgstädt J, Lehner S, Jovic M, Rentsch D, Bülbül E, Huch A, Altenried S, Rend Q, Rupper P, Annaheim S, Gaan S (2021) In-situ phosphine oxide physical networks: A facile strategy to achieve durable flame retardant and antimicrobial treatments of cellulose. Chem Eng J 417:128028. https://doi.org/10.1016/j.cej.2020.128028

Peng C, Li J, Wu Z, Peng W, Zhou D (2016) Investigating into the liquid oxygen compatibility of a modified epoxy resin containing silicon/phosphorus and its mechanical behavior at cryogenic temperature. RSC Adv 6(44):38300–38309. https://doi.org/10.1039/C6RA06033A

Perret B, Schartel B, Stöß K, Ciesielski M, Diederichs J, Döring M, Krämer J, Altstädt V (2011a) A new halogen-free flame retardant based on 9, 10-dihydro-9-oxa-10-phosphaphenanthrene-10-oxide for epoxy resins and their carbon fiber composites for the automotive and aviation industries. Macromol Mater Eng 296(1):14–30. https://doi.org/10.1002/mame.201000242

Perret B, Schartel B, Stöß K, Ciesielski M, Diederichs J, Döring M, Krämer J, Altstaädt V (2011b) Novel DOPO-based flame retardants in high-performance carbon fibre epoxy composites for aviation. Eur Polym J 47(5):1081–1089. https://doi.org/10.1016/j.eurpolymj.2011.02.008

Qian X, Pan H, Xing X, Song L, Yuen R, Hu Y (2012) Thermal properties of novel DOPO-based organic inorganic hybrid materials prepared by sol-gel and UV-curing processes. Ind Eng Chem Res 51:85–94. https://doi.org/10.1021/ie2017493

Qian X, Song L, Hu Y, Yuen RK (2013) Thermal degradation and flammability of novel organic/inorganic epoxy hybrids containing organophosphorus-modified oligosiloxane. Thermochim Acta 552:87–97. https://doi.org/10.1016/j.tca.2012.11.010

Sahyoun J, Bounor-Legare V, Ferry L, Sonnier R, Da Cruz-Boisson F, Melis F, Bonhommé A, Cassagnau P (2015) Synthesis of a new organophosphorous alkoxysilane precursor and its effect on the thermal and fire behavior of a PA66/PA6 copolymer. Eur Polym J 66:352–366. https://doi.org/10.1016/j.eurpolymj.2015.02.036

Saito T (1972) Cyclic organophosphorus compounds and process for making same. US Patent 3,702,878

Salmeia KA, Gaan S, Malucell G (2016) Recent advances for flame retardancy of textiles based on phosphorus chemistry. Polymers 8(9):319. https://doi.org/10.3390/polym8090319

Schäfer A, Seibold S, Lohstroh W, Walter O, Döring M (2007) Synthesis and properties of flame-retardant epoxy resins based on DOPO and one of its analog DPPO. J Appl Polym Sci 105(2):685–696. https://doi.org/10.1002/app.26073

Schartel B (2010) Phosphorus-based flame retardancy mechanisms-old hat or a starting point for future development? Mater 3(10):4710–4745. https://doi.org/10.3390/ma3104710

Schulze T (2006) MassBank available online: https://massbank.eu/MassBank/. Accessed 10 May 2022

Šehić A, Tomšič B, Jerman I, Vasiljević J, Medved J, Simončič B (2016) Synergistic inhibitory action of P-and Si-containing precursors in sol–gel coatings on the thermal degradation of polyamide 6. Polym Degrad Stab 128:245–252. https://doi.org/10.1016/j.polymdegradstab.2016.03.026

Shafizadeh F (1968) Pyrolysis and combustion of cellulosic materials. Advances in carbohydrate chemistry, vol 23. Elsevier, pp 419–474. https://doi.org/10.1016/S0096-5332(08)60173-3

Shen D, Gu S (2009) The mechanism for thermal decomposition of cellulose and its main products. Bioresour Technol 100(24):6496–6504. https://doi.org/10.1016/j.biortech.2009.06.095

Tsuge S, Ohtani H, Watanabe C (2011) Pyrolysis-GC/MS data book of synthetic polymers: pyrograms, thermograms and MS of pyrolyzates. Elsevier

Vasiljević J, Jerman I, Jakša G, Alongi J, Malucelli G, Zorko M, Tomšič B, Simončič B (2015) Functionalization of cellulose fibres with DOPO-polysilsesquioxane flame retardant nanocoating. Cellulose 22(3):1893–1910. https://doi.org/10.1007/s10570-015-0599-x

Vasiljević J, Čolović M, Jerman I, Simončič B, Demšar A, Samaki Y, Šobak M, Šest E, Golja B, Leskovšek M et al (2019) In situ prepared polyamide 6/DOPO-derivative nanocomposite for melt-spinning of flame retardant textile filaments. Polym Degrad Stab 166:50–59. https://doi.org/10.1016/j.polymdegradstab.2019.05.011

Wang X, Hu Y, Song L, Xing W, Lu H, Lv P, Jie G (2011) Effect of a triazine ring-containing charring agent on

fire retardancy and thermal degradation of intumescent flame retardant epoxy resins. Polym Adv Technol 22(12):2480–2487. https://doi.org/10.1002/pat.1788

Wang S, Sui X, Li Y, Li J, Xu H, Zhong Y, Zahng L, Mao Z (2016) Durable flame retardant finishing of cotton fabrics with organosilicon functionalized cyclotriphosphazene. Polym Degrad Stab 128:22–28. https://doi.org/10.1016/j.polymdegradstab.2016.02.009

Weinert M, Döring M (2021) N-phosphorylated iminophosphoranes based on 9, 10-dihydro-9-oxa-10-phosphaphenanthrene-10-oxide and their flame-retardant behavior in epoxy resins. J Appl Polym Sci 138(9):49902. https://doi.org/10.1002/app.49902

Wenig P, Odermatt J (2010) OpenChrom: a cross-platform open source software for the mass spectrometric analysis of chromatographic data. BMC Bioinform 11(1):1–9. https://doi.org/10.1186/1471-2105-11-405

Wiley and Sons Inc. (2000) SpectraBase. https://spectrabase.com/. Accessed 10 May 2022

William EW (2022) Mass Spectra. In: Linstrom PJ, Mallard WG (eds) NIST Chemistry WebBook, NIST Standard Reference Database Number 69, National Institute of Standards and Technology, Gaithersburg MD, 20899. https://doi.org/10.18434/T4D303. Accessed 1 Jun 2022

Wu Q, Sisqueira Curto Valle RC, Borges Valle JA, Maesta Bezerra F, Meng X, Lis Arias MJ (2020) Recent progress of DOPO-containing compounds as flame retardants for versatile polymeric materials. World J Text Eng Technol 6:89–103. https://doi.org/10.31437/2415-5489.2020.06.7

Xie W, Huang S, Tang D, Liu S, Zhao J (2020) Synthesis of a furfural-based DOPO-containing co-curing agent for fire-safe epoxy resins. RSC Adv 10(4):1956–1965. https://doi.org/10.1039/C9RA06425G

Xu Q, Mensah RA, Jin C, Jiang L (2022) A critical review of the methods and applications of microscale combustion calorimetry for material flammability assessment. J Therm Anal Calorim 147(11):6001–6013. https://doi.org/10.1007/s10973-021-10963-4

Yu D, Liu W, Liu Y (2010) Synthesis, thermal properties, and flame retardance of phosphorus-containing epoxy-silica hybrid resins. Polym Compos 31(2):334–339. https://doi.org/10.1002/pc.20809

Zhang J, Mi X, Chen S, Xu Z, Zhang D, Miao M, Wang J (2020a) A bio-based hyper-branched flame retardant for epoxy resins. Chem Eng J 381:122719. https://doi.org/10.1016/j.cej.2019.122719

Zhang W, Yang R (2011) Synthesis of phosphorus-containing polyhedral oligomeric silsesquioxanes via hydrolytic condensation of a modified silane. J Appl Polym Sci 122(5):3383–3389. https://doi.org/10.1002/app.34471

Zhang W, Li X, Yang R (2011) Novel flame retardancy effects of DOPO-POSS on epoxy resins. Polym Degrad Stab 96(12):2167–2173. https://doi.org/10.1016/j.polymdegradstab.2011.09.016

Zhang Z, Yuan L, Liang G, Gu A (2016a) Fabrication and origin of flame retarding glass fiber/bismaleimide resin composites with high thermal stability, good mechanical properties, and a low dielectric constant and loss for high frequency copper clad laminates. RSC Adv 6(24):19638–19646. https://doi.org/10.1039/C6RA00067C

Zhang Z, Yuan L, Liang G, Gu A (2016b) A strategy and mechanism of fabricating flame retarding glass fiber fabric reinforced vinyl ester composites with simultaneously improved thermal stability, impact and interlaminar shear strengths. Polym Degrad Stab 125:49–58. https://doi.org/10.1016/j.polymdegradstab.2016.01.002

Zhang Z, Dong C, Liu J, Kong D, Sun L, Lu Z (2020b) Preparation of a synergistic reactive flame retardant based on silicon, phosphorus and nitrogen and its application to cotton fabrics. Cellulose 27(3):1799–1815. https://doi.org/10.1007/s10570-019-02900-4

Zilke O, Ali W, Kamps L, Engels T, Schumacher S, Danielsiek D, Shabani V, Salma A, Plohl D, Wallmeier R, Opwis K, Gutmann JS, Mayer-Gall T (2022) Water-Soluble cyclophosphazenes as durable flame-retardant finishes for nylon/cotton blend fabrics. ACS Appl Polym Mater. https://doi.org/10.1021/acsapm.2c01257